Cellulose and Chitin Twisted Structures: From Nature to Applications

Rafaela da Rosa, Susete Fernandes, Michel Mitov, Maria Helena Godinho

Adv. Funct. Mater, 2304286 (2023) — Accepted version

Cellulose and chitin twisted structures: from nature to applications

Rafaela R. da Rosa, Susete N. Fernandes, Michel Mitov and Maria Helena Godinho**

Rafaela R. da Rosa, Susete N. Fernandes and Maria Helena Godinho
i3N|CENIMAT, Department of Materials Science, NOVA School of Science and Technology, NOVA University Lisbon, Campus de Caparica, Caparica 2829-516, Portugal
E-mail: mhg@fct.unl.pt; sm.fernandes@fct.unl.pt

Michel Mitov
Université Côte d'Azur, CNRS, Institut de Physique de Nice, INPHYNI, 17 rue Julien-Lauprêtre, F-06200 Nice, France
E-mail: michel.mitov@univ-cotedazur.fr

Keywords: cellulose, chitin, twisted structures

Twisted structures are ubiquitous in plants and animals. Cellulose and chitin are natural polymers that form the structural skeleton of various twisted systems observed across different length scales, ranging from the molecular to the nano, micro, and macro scale. In addition, cellulose and chitin helicoidal structures were found to be responsible for structural coloration, enhanced mechanical properties, and motion. This review first addresses cellulose and chitin-based chiral molecular systems and nanoscale helicoidal arrangements. Attention is given to cellulose nanocrystals, water interactions, out-of-equilibrium structural colorful structures formed by cellulose derivatives, and chitin's optical and mechanical properties.

The discussion progresses to the micro and millimeter scales, where specific examples are presented to showcase specialized helical cellulose-based organizations. The chosen examples illustrate the formation of different helicities, adaptative shapes, and movements at varying length scales, such as in vascular leaf petioles at the micro-scale and millimeter-scale in tendrils and awns of *Erodium* fruits. So far, the results indicate that significant work should be done on out-of-equilibrium systems. In addition, much must be learned from nature to produce novel twisted functional materials. This work aims to provide a comprehensive overview of the state-of-the-art study of twisted cellulose and chitin-based structures and their potential applications.

https://doi.org/10.1002/adfm.202304286

Received: April 18, 2023.
Revised: June 28, 2023.
Accepted: June 30, 2023.

1. Introduction

Cellulose and chitin are carbohydrates that play important structural roles in living organisms. While plants are the most abundant source of cellulose, chitin in the animal world is the second most abundant polysaccharide after cellulose. Cellulose exists in the cell walls of plants, forming their structural component (skeletal support system) as anisotropic aggregates (nanocrystals, microfibrils, or fibrils). At the molecular level, cellulose comprises repeating glucose units connected by β(1→4)-glycosidic bonds in a linear chain.[1] The orientation of these chains relative to each other gives rise to the characteristic helical structure of cellulose. This chirality is further manifested at larger scales as cellulose chains aggregate.[2] However, the handedness of the cellulose-based structures at different length scales can differ from the chirality of the main cellulose chain at the molecular level indicating that cellulosic helical structures appear due to other mechanisms than the chirality of cellulose. Some examples from the macro- to the microscale include the trunks of the trees that can be right-handed, left-handed, or untwisted; The helical shapes of tendrils existing in climbing plants, for instance, in *Passiflora edulis* (**Figure 1**a and 1b),[3] that can turn left and right along the same filament (Figure 1a); The cell walls of plants that can possess right-handed and left-handed helicoidal structures, at the nanoscale, as the known example exhibiting brilliant and iridescent colors *Pollia condensata* fruit (Figure 1c);[4,5] *Erodium* belonging to the *Geraniaceae* plant family possess humidity responsive awns that can switch from straight configurations when wet (Figure 1d) to right-handed helices (R) in the dry state (Figure 1e);[6] The helical left-handed microfilaments in the xylem vessels of plants leaves (Figure 1f and 1g).[7]

Chitin is mainly found in the exoskeletons or cuticles of arthropods — *i.e.*, in the carapace of crustaceans[8] (Figure 1h), insects[9] (Figure 1i), myriapods and arachnids –, the cell walls of fungi and the cartilage of mollusks;[10] the development of our knowledge about chitin throughout the 220 years of its history is reviewed in reference [11]. Chitin is a glucose derivative consisting of a long-chain polymer of (1,4)-β-*N*-acetylglucosamine units,[12,13] forming, as cellulose, hierarchical structures from the nano to the macroscale.

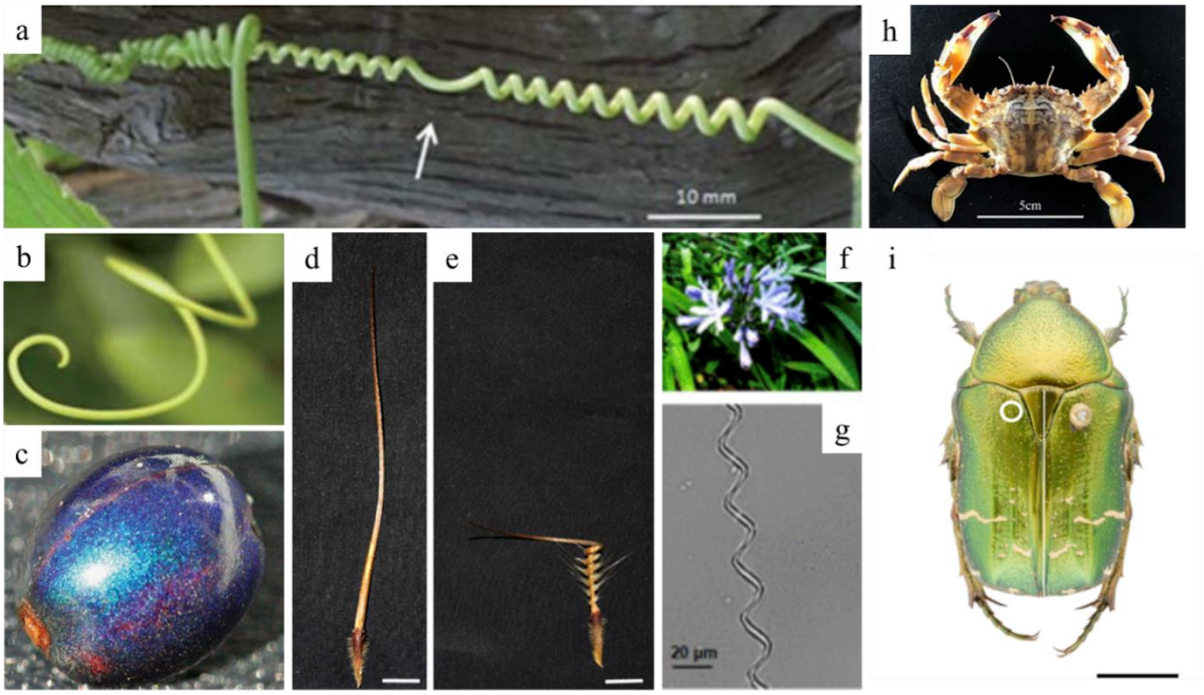

Figure 1. Twisted cellulose and chitin-based structures in animals and plants: a) *Passiflora edulis* tendrils supported by both ends showing right and left-handed helices separated by a straight segment, indicated by the white arrow, and b) spiral from a tendril supported by one end. Used with permission of The Royal Society of Chemistry, from [3] Copyright © 2010; permission conveyed through Copyright Clearance Center, Inc. c) Bluish pixelated *Polia Condensata* fruit. Reproduced under the terms of the CC BY 3.0 license.[5] Copyright © 2014, The Authors, published by WILEY-VCH Verlag GmbH & Co. KGaA, Weinheim. d) Straight wet and e) Right-handed dried, *Erodium gruinum* awn. Reprinted with permission from ref. [6] Copyright 2012 by the American Physical Society. f) *Agapantus africanus* flower and leaves. g) Left-handed microfilament existing in the xylem vessel of *Agapantus africanus* leaves. Adapted with permission from [7]. Copyright © 2014, American Chemical Society. h) The exoskeleton of *Charybdis japonica* is an example in which a helicoidal chitin structure can be found. Reproduced under the terms of the CC BY 4.0 license.[8] Copyright © 2022, The Authors, published by Springer Nature. i) Bright structural coloration in the carapace of *C. aurata* beetle, scale bar represents 0.5 cm. Reprinted from [9], Copyright © 2018, with permission from Elsevier.

Cellulose and chitin self-assembled helicoidal main chain polymer molecules and nanorods, such as in plant cell walls and skeletal structures, resemble chiral nematic (cholesteric) liquid crystalline phases with no fluid characteristics. In this sense, we dedicate the following section to liquid crystalline (LC) phases and the relationship between the structures found in helicoidal LCs and biological systems.

Then we will look at cholesteric structures in plants responsible for coloration and how water interactions can affect these structures. Recent results related to coloration by self-assembling in cellulosic systems, namely cellulose nanocrystals (CNCs)/water and cellulose derivatives, will be addressed, as how these structural colors can be affected by water interactions and out-

of-equilibrium systems. The following sections will explore the twisted plywood chitin Bouligand structures found in some organisms and their optical and extraordinary mechanical properties.

Finally, at the micro and millimeter scales, cellulose-based left-handed micro helices from vascular leaf petioles, tendrils with both left and right-handed helices, and movements observed in helical plants' awns will be addressed along with some applications.

2. Biological helicoidal liquid crystalline systems

Assemblies of nano and micro cellulose fibers are at the genesis of typical series of arced patterns that can be observed in sections of the cell wall of the plants (**Figure 2**a and 2e).[14,15] Similarly, the insect's cuticle shows hierarchical patterns made of chitin fibers with protein molecules. A succession of nested arcs was observed in the crab cuticles in cytoplasmic inclusions, the organic matrix of several animal skeletal structures, in Invertebrates, in the nucleus of many Bacteria, and in the Dinoflagellate chromosomes.[16] Multifunctionality arises from this structural complexity and avoids chemical diversity, allowing a sustainable saving of materials and favoring recycling.[17]

Drach, in 1951,[18] tried to explain the arced structures observed in the cuticle of a Crustaceans, *Decapod Reptantia*, using phase contrast and electronic microscopy. The model developed by Drach involved the existence of curved fibers that joined successive layers of chitin. Bouligand, in 1965,[19] showed that this model could not interpret the experimental results obtained for arced patterns observed in the skeleton of many Arthropods (Figure 2a).[14,19] Yves Bouligand showed that these patterns reveal a liquid crystalline structure of fibers throughout the cuticle.[20] Bouligand's model is based on several equidistant planes that contain molecules, represented by straight lines, that rotate from one plane to the next by a slight and constant angle. Half of the pitch of the helicoidal structure corresponds to a rotation of 180º of the whole planes (or the rotation of the molecular directions in the planes). The observation of this structure in planes oblique to the helical axis reveals a series of parallel nested arcs, as highlighted in Figure 2a. The helicoidal structure inferred from experimental results was justified by the variation of the orientation of the parabolas in sections cut at different angles, by the presence of discrete lengths of the constituent fibers, and by the optical activity of structures with arced patterns found in many scarab beetles.[21] Neville, 1976, used the helicoidal model to explain the arced architectures found in the cell wall of *Chara vulgaris* oospores (Figure 2a and 2e).[15]

Different types of twisted structures were identified in biological systems depending on the organization of the twisted plywood structure involving flat, coaxial cylinders, and toroidal geometries that imposes planar, cylindrical, and toroidal twist, respectively.[22]

The supramolecular organizations of cellulose in the cell walls resemble helicoidal liquid crystalline structures but in dense consolidated solid structures. The solidification of the mesomorphic helicoidal structures happens, according to Bouligand,[20,22] via covalent crosslinks that occur gradually in skeletal structures, and the term pseudomorphosis was introduced in 1972[20] to designate these anisotropic structures that do not exhibit the rheological properties characteristic of the fluids. In insects, sclerotization is a chitin matrix crosslinking reaction that increases the rigidity of the cuticle; insect growth and morphogenesis depend on the capability to remodel chitin structures. The mineralization of the chitin matrix by calcium and magnesium carbonates solidifies the matrix in crustaceans.[23] The twisted plywood is continuous, like a synthetic liquid crystalline structure, and not stratified. The planes are virtual and have no physical meaning.[24,25]

Next, a description of liquid crystalline phases is outlined to understand better the self-assembled helicoidal structures in cellulose and chitin-based systems.

Liquid crystals or mesophases exist between the isotropic liquid and the crystalline phase exhibiting the liquids' fluidity and the crystals' anisotropy.[26–28] Mesomorphic substances are subdivided into two main types, depending on how they can be obtained; thermotropic, which presents, through a thermal process, one or more mesophases (polymorphism), and lyotropic, which displays mesomorphic behavior in an appropriate solvent, within a given range of concentration, pressure, and temperature. The anisometric shape of the constituent molecules also characterizes the liquid crystalline phases. This review paper will refer to mesophases formed by rod-like shape entities and polymeric mesophases made of semi-rigid or rigid chains containing mesogenic parts. Liquid crystals are also characterized by different structures, including the nematic, the smectic, and the cholesteric (chiral nematic) phases. In uniaxial nematic phases, the calamitic molecules present the centers of mass randomly distributed, with no positional order, in the same manner as in an isotropic fluid. However, simultaneously, the uniaxial nematic phase presents a long-range orientational order. The uniaxial nematic phase is characterized by the quadrupolar uniaxial order parameter $S_{ij} = S\left(n_{ij} - \frac{1}{3}\delta_{ij}\right)$ in which the unit vector **n**, called director, is parallel to the common orientation of molecules, S represents the amplitude of the orientational order that varies between 0 in the isotropic phase and +1 in the perfectly oriented phase.[27,28] In the smectic phase, which lost one translation degree of freedom

compared to the nematic phase, the molecules remain aligned in one direction but are distributed inside equidistant 2D liquid layers. Depending on the orientation of the rods inside the layers, the distribution of their mass centers, and the thickness of the layers, different types of smectic are obtained. The cholesteric phases are characterized by a helical structure that can be idealized as a twisted nematic along an axis (optical axis) normal to the plane containing the aligned rods. The cholesteric phase or chiral nematic phase is characterized by the pitch P of the helix and the sense of its torsion (left or right-handed). The periodic structure with the pitch P reflects the light (Bragg reflection). The wavelength λ of the light reflected by the structure varies with the pitch, the angle θ, and the refraction index $\bar{n}$, accordingly to the de Vries equation:[29] $\lambda = \bar{n}P$, where θ is the angle between the incident beam and the helix axis of the cholesteric structure. When the pitch is in the visible range (0.4- 0.8 µm), the material is iridescent. For $\theta = 0$, the circularly polarized (CP) light having the same handedness of the helix is reflected, while CP light with opposite handedness is transmitted.

When the incident beam is normal to the helix axis, and the pitch is in the range of 1-100 µm, a characteristic fingerprint texture can be observed under a polarized optical microscope (POM) between crossed polars (Figure 2b and 2c, 2f and 2g).[30–32] The fingerprint texture consists of alternating light and dark bands corresponding to the parallel and perpendicular alignment of the molecules to the plane of the sample preparation. The distance between two light or two dark bands equals to 180º twist of the molecular orientations, i.e., ½ of the cholesteric pitch.

Apart from fingerprints, the cholesteric samples can present other characteristic textures resulting from dislocation and disclination lines (Figure 2d and 2h).[33] While disclinations lines appear in fan-shaped textures, dislocations can be observed in fan-shaped textures, polygonal fields, and planar textures (Figure 2h).[32]

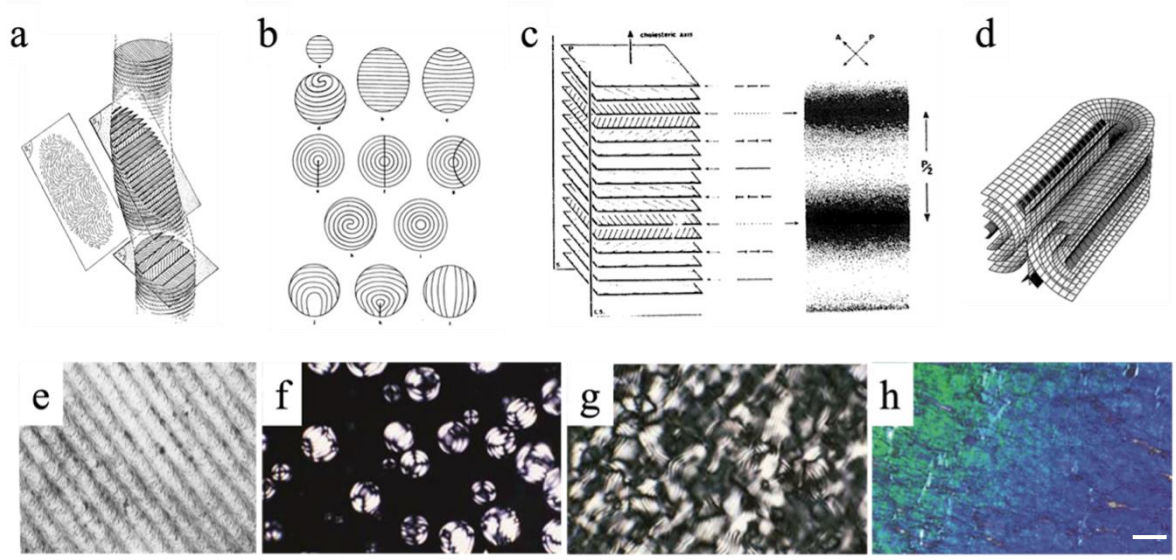

Figure 2. Bouligand, cholesteric structures, and textures: a) Twisted Bouligand structure. Cylinder cut at different angles to the helix axis (S_1 and S_2), a sketch of arcs (S'_1) seen in S_1.[14] Copyright © 1968, Springer-Verlag. Reproduced with permission from SNCSC. b) Schemes of droplets with the homeotropic and planar alignment of the cholesteric layers (represented by lines). The distance between lines represents the 180º rotation of the director, i.e., half of the pitch of the cholesteric helix. Reproduced with permission.[30] Copyright © 1984, EDP Sciences. c) Idealized cholesteric structure with the optical axis parallel to the slide and the cover slide. Between cross polars, alternate white and black bands (fingerprints) can correspond to molecules aligned parallel or perpendicular to the observation plane. Reprinted from [31], Copyright © 1991, with permission from Elsevier. d) Scheme showing an example of an oily streak, a defect that occurs in a cholesteric when molecules align parallel to the slide and cover slide (planar anchoring).[33] Copyright © 2001, Springer-Verlag New York, Inc. Reproduced with permission from SNCSC. e) Arcs appear in an oblique cut of the cell walls of *Chara vulgaris* oospores.[15] Copyright © 1976, Springer-Verlag. Reproduced with permission from SNCSC. f) and g) fingerprints (in f) cholesteric droplets dispersed in an isotropic phase), and h) planar cholesteric structure with oily streaks, between cross polarizers, textures f) to h) are characteristic of cholesteric cellulosic phases. The scale bar represents 2.5 µm.[32] Reprinted by permission of the publisher (Taylor & Francis Ltd).

3. Helicoidal cellulosic structures responsible for colors in plants

The structural color obtained from helicoidal cellulose designs has been observed in different parts of several plant species comprising leaves[34–37] and fruits.[4,38–40] *Mapania caudata*[34] and *Microsorum thailandicum*[36,37] are examples of plants with leaves showing bright structural coloration. The colors observed in the leaves of *Mapania caudata* were associated with a left-handed cellulose helicoidal structure combined with silica grains uniformly distributed in the adaxial epidermal cell wall. The presence of the silica particles in multiple layers was referred to improve the iridescent blue color of the leaves efficiently.[34] The mechanism found by *Mapania caudata* to enhance the coloration of the leaves through the dispersion of silica particles in a helicoidal matrix is an inspiration to produce photonic coatings with selective handedness. For *Microsorum thailandicum*, the photonic behavior of both sides of the leaves was investigated. Different techniques were used, including polarized optical microscopy, transmission electron microscopy, and cryogenic scanning electron microscopy. It was found that the adaxial and abaxial surfaces own left-handed helicoidal cellulose microfibrils structures, with the adaxial side coloration more intense than the one reflected by the abaxial side.[36,37] The existence of cholesteric left-handed structures on both sides of the leaves, with different pitches, suggests that the selective reflection of the left circular component of the polarized light (LCP) and transmission of the right circular polarized light (RCP) could be related to the protection of the plant against photodegradation and harvesting of light.[36] Nevertheless, further research is needed to understand the role of the helicoidal cellulose layers

and to elucidate the origin of the distinct reflection observed in the adaxial cell walls, contrasting to the reflection observed in the abaxial cell walls.

Helicoidal cellulose architectures are also responsible for the vibrant metallic coloration found in some fruits, such as *Margaritaria nobilis*[38] (**Figure 3**a and 3b) and *Pollia condensata*.[4] *Margaritaria nobilis* fruits can be found in Brazil[40] and Mexico.[41] The fruits possess a green exocarp that exposes the inside fruit's blue-metallic color after opening. In Brazil, it was reported that the green exocarp opens on the floor after the fruit has fallen from the tree, while for *Margaritaria nobilis* in Mexico, the capsules open in the tree. Seed birds' dispersal studies made with the fruits from *Margaritaria nobilis* in Brazil indicate that the birds were much more attracted to the blue-metallic color of the fruits in the ground than to the green fruits in the tree. It was reported that only *Turdus leucomelas* was seen to swallow the green fruit, while jays (*Cyanocorax chrysops*), guans (*Penelope superciliaris*), doves (*Geotrygon montana*) and collared peccaries (*Pecari tajacu*) were found to eat the blue metallic units dispersed in the ground.[40] In this way, it was recognized[38,40] that birds seem highly responsible for the dispersion of *Margaritaria nobilis* seeds playing the metallic coloration of the fruit units a relevant role. In 2016 S. Vignolini et al. used light microscopy, scanning and transmission electron microscopy to study *Margaritaria nobilis* fresh fruits. Their work demonstrated the existence of the helicoidal Bouligand multilayer structure in the endocarp of the fruit. The authors also reported changing the metallic blue-green to white as the fruit dried (Figure 3b).[38] The color variation was attributed to an air layer between the helicoidal endocarp structure and the seeds. This layer develops when the seeds shrink due to water removal. The white color was attributed to the air layer that scattered the light, as shown in Figure 3c.[38] The blue coloration was found to reappear when the fruit was rehydrated. It is interesting to follow the variation of the colors of the *Margaritaria nobilis* fruits as they dry. Figure 3b shows an intriguing reddish fruit before the white dried fruit. This also indicates that the mechanisms concerning the development of structural color in nature, as stated by S. Vignolini and al.,[38,39] are still poorly understood. The intense coloration associated with the multilayer and curved geometry of the coating of *Margaritaria nobilis* seeds inspired the production of hollow photonic fibers responsive to different solvents.[42]

Pollia condensata fruits present a pixelated coloration that was first correlated with a cellulose arrangement similar to the Bouligand structure in 2012.[4] The authors also reported that the cellulose helical structures existing in the epidermal cell wall of the same fruit could be right and left-handed. Contrary to the metallic coloration of *Margaritaria nobilis* fruits, which

changes with humidity, the intense blue coloration and pixelated features of *Pollia condensata* fruits persist when the fruit dries.

Recent studies[43] address the formation of the helicoidal colored structures in Pollia japonica fruits and understanding of the underlying mechanisms responsible for their appearance. Noninvasive and nondestructive optical techniques were used to follow and measured structural modifications of the helicoidal cell wall structures over a period of one month. Four stages of development were identified based on the visual coloration of the fruits, as shown in Figure 3e to 3h.[43] Contrary to the fruits of *Pollia condensata*, the fruits from *Pollia japonica* were reported to display only left-handed helicoidal cellulose arrangements. Moreover, the variation of the colors at the macroscale corresponds to the same value of the pitch of the helicoidal cellulose structure at the micro/nanoscale. The authors also concluded that the helicoidal deposition of the cellulose nanorods should mainly be influenced by the chemical composition of the cell wall and less by the reorientation promoted by mechanical constraints due to water removal and compression. Indicating that the sequence of colors observed over time needs a deeper understanding and further investigation.

The following two sections focus on creating structures derived from liquid crystalline phases of cellulose nanocrystals and cellulose derivatives. Specially, we will explore the impact of water and non-equilibrium systems on forming cellulose-based helicoidal structures with distinct colors.

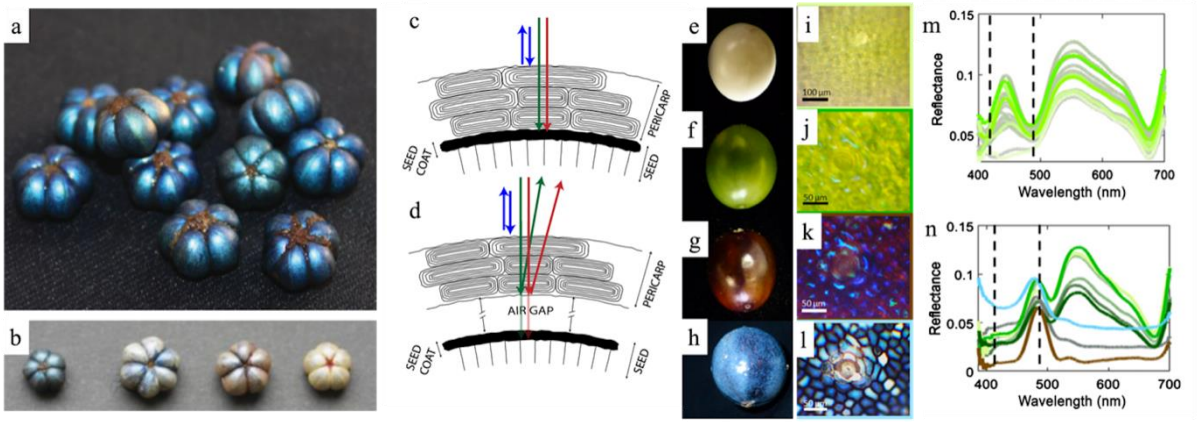

Figure 3. Evolving iridescence in fruits a) *Margaritaria nobilis* fruits showing the blue-metallic color of the inside fruit after opening the green exocarp. b) Development of the color and shape as the fruits dehydrate from blue to white, respectively. Scale bar 1 cm.[38] c) and d) Cross section of *Margaritaria nobilis* wet and dry pericarp, respectively, according to reference [38]. Reproduced under the terms of the CC BY 4.0 license.[38] Copyright © 2016, The Authors, published by the Royal Society. e) to h) Maturation stages of *Pollia japonica* fruits according to reference [43]. i) to l) optical microscopy photos, between cross polarizers, respectively.[43] m) Reflection spectra of LCP light showing the evolution of the fruit color from white to blue according to images e) to h) and i) to l). Reproduced under the terms of the CC BY 4.0 license.[43] Copyright © 2021, The Authors, published by John Wiley and Sons.

4. Cellulose water interactions and liquid crystalline phase formation

In systems ranging from the nano to molecular scale (**Figure 4**a), the water interactions with cellulose chains play an important role in the liquid crystalline phase formation, although their complexity gets often neglected.[44,45] Cellulose synthesis occurs at the plasma membrane of plant cells (Figure 4b and 4c).[46–50] The nascent polysaccharide is synthesized by an enzyme called cellulose synthase (CesA), which is arranged in a trimeric configuration (Figure 4b), producing chains that subsequently aggregate into protofibrils. These protofibrils are the genesis of microfibrils, being assembled by the rosette (hexameric organization of CesA trimers).[2] Recent work demonstrates that water molecules play an essential role in the cellulose biosynthesis mechanism during the polymerization step.[51]

Molecular dynamics (MD) and atomistic simulations have been valuable tools for investigating the role of water in cellulose interactions, alignment, and twist[52–59]. Nonetheless, to our knowledge, no research has investigated the presence of water during the protofibril to microfibril aggregation and alignment, being the latter considered the elementary crystalline structure of cellulose.

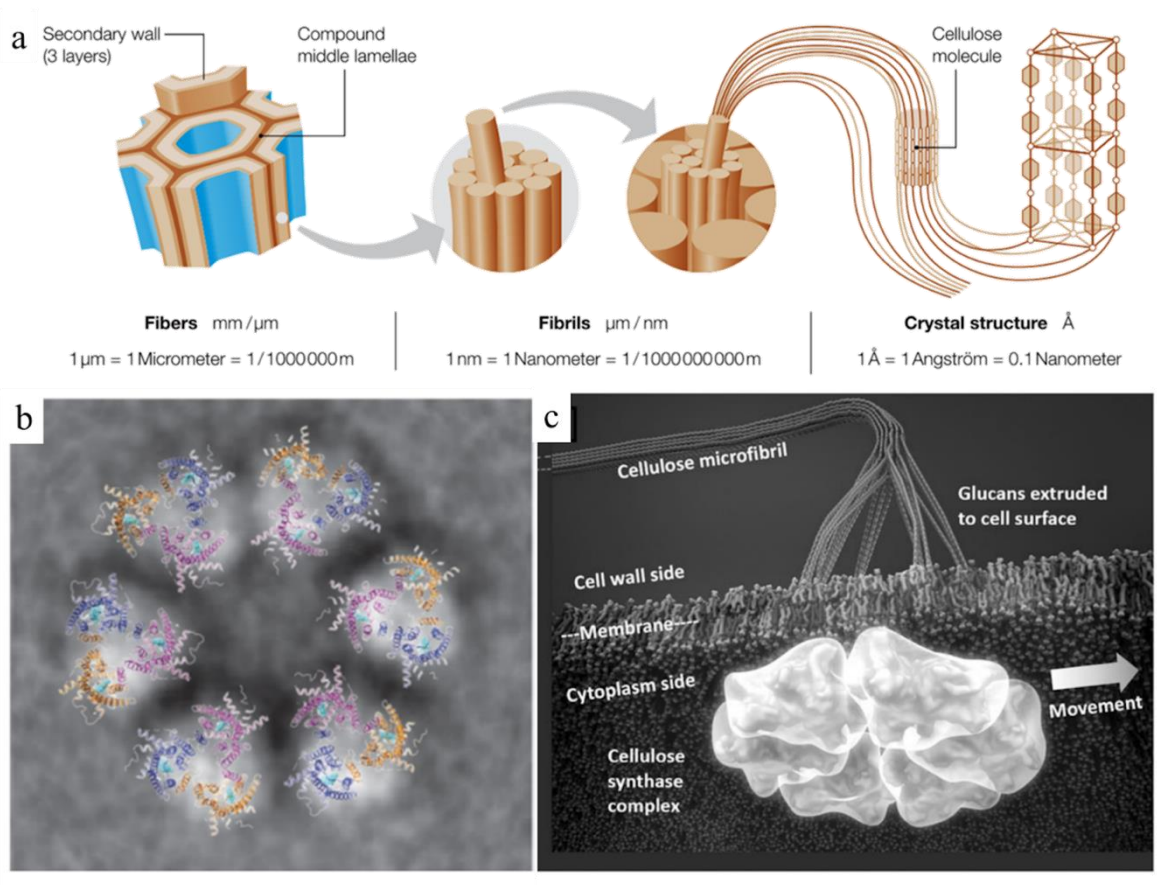

Figure 4. Cellulose biosynthesis towards cell wall formation. a) Plant cell wall hierarchy. Reproduced with permission.[60] Copyright © 2004, WILEY-VCH Verlag GmbH & Co. KGaA, Weinheim. b) Hexameric organization of CesA trimers comprising the rosette. From [2]. Reprinted with permission from AAAS. c) Artistic rendition of a cellulose synthase complex embedded in a plasma membrane during microfibril synthesis. Reproduced under the terms of the CC BY 4.0 license.[50] Copyright © 2022, The Author, published by Oxford University Press on behalf of American Society of Plant Biologists.

Recent MD simulations have demonstrated that introducing water molecules at the interior microfibril interfaces results in a lower free energy state compared to the reference state where no water is present between the microfibrils (**Figure 5**a).[61] In addition, various types of water which interact differently with cellulose chains depending on the surface between and within the microfibril bundle or aggregates are known. This feature is associated with both mobile and immobile water environments.[62]

The water molecule hydrogen bonding with the crystal surface has a minimal effect on cellulose twisting.[57] However, studies have shown that the water molecule can impact the polymer conformation if an intramolecular hydrogen bond between two glycosidic units is broken to form new intermolecular ones with water (Figure 5b).[55] The water effect may translate into more or less twisting of the cellulose molecule.[55]

The interplay between chirality, water, and materials is a complex topic that demands further research and investigation. While there are some observations and correlations, there is still much to uncover about the fundamental nature of these phenomena and how they interact.

The microstructure in the crystalline elementary fibril (microfibril) theory, characterized by strains-distorted tilted and twisted regions, makes them easily accessible (Figure 5c).[63] Consequently, these regions can be readily hydrolyzed, releasing rod-shaped cellulose nanocrystals (CNCs).[64,65] Acid hydrolysis is the most used method for CNCs production due to its simplicity and high yield. Although sulfuric acid is the most used reagent (Figure 5d), hydrochloric and phosphoric acids have also been utilized.

During acid hydrolysis, the acid protonates the oxygen atoms in the glycosidic bonds of cellulose in the disordered regions of the microfibril, which weakens the bond and promotes its cleavage.[66,67] As a result, enhanced electrostatic stabilization is achieved in the suspension due to introduction of sulfate half-ester groups on the cellulose crystallite's surface.[68] Introducing such groups with high electronic density on the surface of CNCs plays a crucial role in colloidal stability.[69] The sulfate half-ester groups repel each other due to their negative charges, preventing the CNCs from aggregating and causing precipitation. In addition, the presence of

these groups also facilitated the dispersion of the CNCs in aqueous solutions, as they interacted favorably with water molecules.

These suspensions of highly polydisperse rod-like colloids exhibit significant deviations from Raoult's law and may separate into phases depending on the diameter (D) and length (L) values. Onsager[70] predicted that a high aspect ratio (L/D) colloidal anisometric particles could form liquid crystalline phases. When the anisotropic (LC) and isotropic (I) phases coexist, the volume fractions (Φ) of both phases can be calculated using the following equations: $\Phi_{LC} = 4.2$ D/L and $\Phi_I = 3.3$ D/L.

The reason for the long-range alignment of nematic nanorod suspensions is that the ordering arises from entropic effects. Specially, the gain in translational entropy that results from rods aligning along a common direction compensates for the loss in orientational entropy. This alignment enables the rods to move freely over long distances without being hindered by other rods, thus increasing their overall translational freedom. The system´s free energy is reduced, making nematic order appear as a result.

Although the theory relates nematic LC phase formation for flat rod-like colloids, it cannot explain the twist observed during the chiral nematic phase formation. Revol, in 1992, predicted that the nanorods of both chitin and cellulose would be right-handed twisted structures (Figure 5e) based on the demonstration of left-handed liquid crystalline phase formation of both nanocrystal suspensions.[64,71]

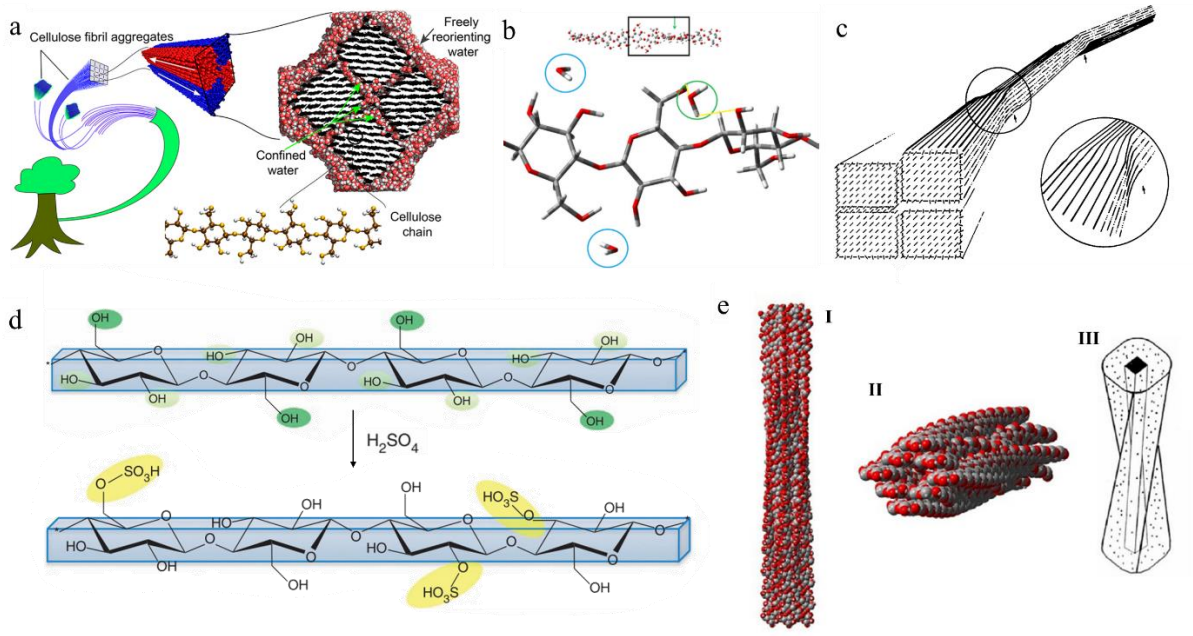

Figure 5. Water interactions and twist in cellulose at different length scales. a) Interior microfibril interfaces interacting with water resulting in a lower free energy state. Reproduced under the terms of the CC BY 4.0 license.[61] Copyright © 2022, The Authors published by American Chemical Society. b) A hydrogen bond through the glycosidic bond. The green-

circled water molecule can form a hydrogen bond with close hydroxyl groups, which affects the glucose units rotation. On the other hand, the blue-circled water molecules do not affect the twist, although they interact with cellulose. Reprinted from ref. [55], Copyright © 2015, with permission from Elsevier. c) Strains-distorted tilted and twist regions. Reproduced with permission.[63] Copyright © 1972, John Wiley & Sons, Inc. d) Schematic representation of half-ester groups on the CNC surface after acid hydrolysis using H_2SO_4.[72] Copyright © 2014, The Author(s), published by Springer Nature. Adapted with permission from SNCSC. e) A right-handed twisted crystalloid. Adapted from [55], Copyright © 2016, with permission from Elsevier.

The process of phase separation from an initially isotropic suspension begins with phase nucleation at various points of the isotropic phase, forming anisotropic microdroplets. It requires a balance of attractive forces to assemble the mesogens into tiny droplets and repulsive forces to arrange mesogens into a liquid crystalline order.[73–75] The observation of the anisotropic spindle-like shape domains was first reported in 1925 in a suspension of needle-like crystals of vanadium pentoxide,[76] commonly seen in nematic phases from colloidal particles.[77–79] In the same work, they demonstrate that a more concentrated fraction of the same system forms large homogeneous anisotropic patches in which only biangular holes are filled by the isotropic suspension. The term tactoid (*taktoide*) was introduced later[80] to describe the drops of anisotropic sol (*taktosol*) in the isotropic sol (*ataktosol*). As an analogy, they termed the drops of isotropic sol in an anisotropic sol as atactoid or negative tactoid (*ataktoide* or *negative taktoide*) (**Figure 6**a and 6b).[81]

Due to the rod-like shape of CNCs, their colloidal suspensions also usually undergo a phase separation into an atop isotropic and a bottom anisotropic phase. In 1992, the spontaneous formation of small tactoids with chiral nematic order was observed for the first time, resulting in an anisotropic phase formation (Figure 6c).[64] The chiral nematic tactoids coalesce, increasing the bottom anisotropic phase volume fraction to form a cholesteric phase (Figure 6d) with only a left-handed helicoidal arrangement.[82,83] Solid iridescent films with Bouligand-resembling structures can be obtained upon drying.[72,84,85]

Cholesteric tactoids formed in CNC suspensions are spherical or ellipsoidal microdroplets. Fingerprint texture can be seen on the tactoid if weak or homeotropic CNCs anchoring is established at the biphase interface, usually observed for CNC liquid crystalline colloidal suspensions.[73]

An efficient method was achieved to capture the tactoids formed in CNC aqueous suspensions. Using electron microscopy, the CNCs organization was directly observed at the nanoscale from tactoids stabilized into a solid matrix.[86] Different-sized tactoids presented distinct CNC

arrangements. In the small captured tactoids, the CNCs are uniformly aligned due to the boundary conditions, so they appear as unwound nematic. In contrast, a series of periodic bands are observed for the larger tactoids, with a left-handed cholesteric structure.[73]

During the coalescence process (Figure 6e), where the fusion of smaller tactoids affords larger ones, the combination of initially random orientation in the microdomains causes the director field topological defects of the resulting tactoid. The thermodynamically unstable defects could be healed by the director's field reorientation. The cholesteric phase nucleation and growth were observed to be substantially influenced by the boundary conditions, by analyzing the topological defects and liquid crystalline tactoids evolution of the suspensions in the geometrical confinemet of nonspherical droplets.[87]

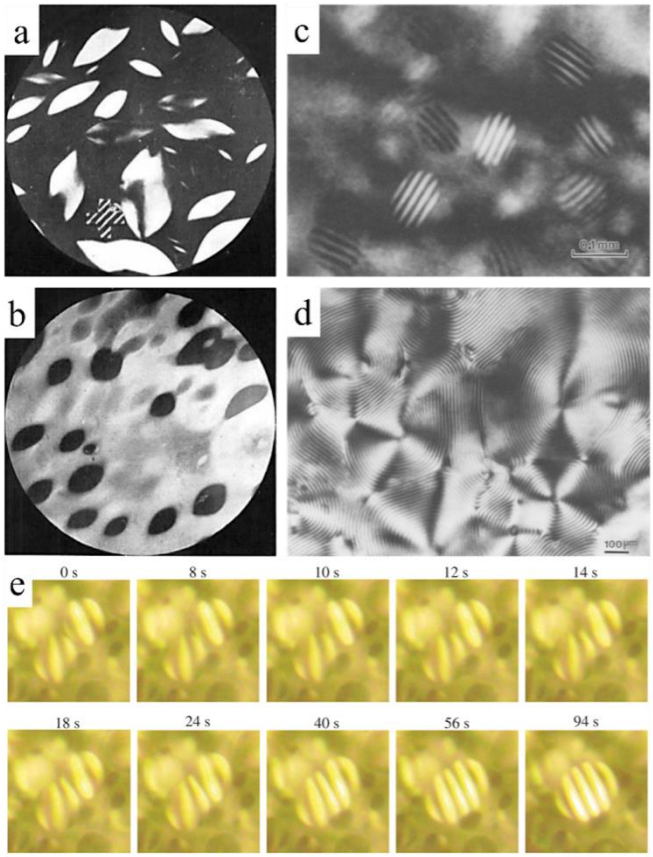

Figure 6. Phase nucleation and time evolution of tactoid coalescence. a) Vanadium pentoxide suspensions with different concentrations forming tactoids and b) atactoids. Reproduced with permission.[76] . Copyright © 1925, John Wiley & Sons, Inc. c) Chiral tactoids formation from CNC suspension and d) cholesteric phase formation after phase separation. c-d) Reprinted from [64], Copyright © 1992, with permission from Elsevier. e) Time evolution of chiral nematic tactoids coalescence. Used with permission of The Royal Society (U.K.), from [73]; permission conveyed through Copyright Clearance Center, Inc.

Although the colloidal suspensions of CNCs form cholesteric phases after chiral nematic tactoids coalescence,[64] the source of chirality in CNCs suspensions is still under debate.[88–90] It has been shown in a recent work an unusual behavior of density phase inversion (**Figure 7**a).[91] It was reported for the first time the formation of atactoids (Figure 7b) in CNC aqueous suspensions. The authors pointed out the crucial role of water in never dried sources during the freeze-thaw step before the dialysis. They suggested that the entrapped water within CNCs freezes out, leaving the air inside the nanoparticle~~'s~~ structure. Thus, the anisotropic phase of the interacting nanorods turns less dense than water and separates into an upper anisotropic phase and a bottom isotropic phase (Figure 7a). A change in chain conformation was also suggested based on XPS and contact angle experiments. The water behavior was also demonstrated to be different by ^{1}H NMR relaxometry in the upper LC phase compared with the usual high-density one (Figure 7c). In contrast, the low-density LC phase forms atactoids (Figure 7b) instead of tactoids (Figure 7d), which phenomena remains to be addressed.

As stated above, cellulose nanocrystals (CNCs) exist in different plants' cell walls. They can be responsible for their spectacular bright iridescent coloration when isolated and, above a critical concentration in water, can form a left-handed cholesteric phase.[92] It was demonstrated that the water evaporation rate upon CNC film drying affects the properties of the photonic film (Figure 7e).[93,94] It was also shown that a new approach for patterning CNC films produces materials with drastically different optical properties by changing the time of water evaporation across distinct zones of a drying CNC colloidal suspension (Figure 7f).[94] With careful drying rate control during the casting process, an inverse relationship between the evaporation rate and the pitch and its uniformity is observed, thus leading to a larger pitch upon rapid evaporation and a more significant disordered structure in the film.[85]

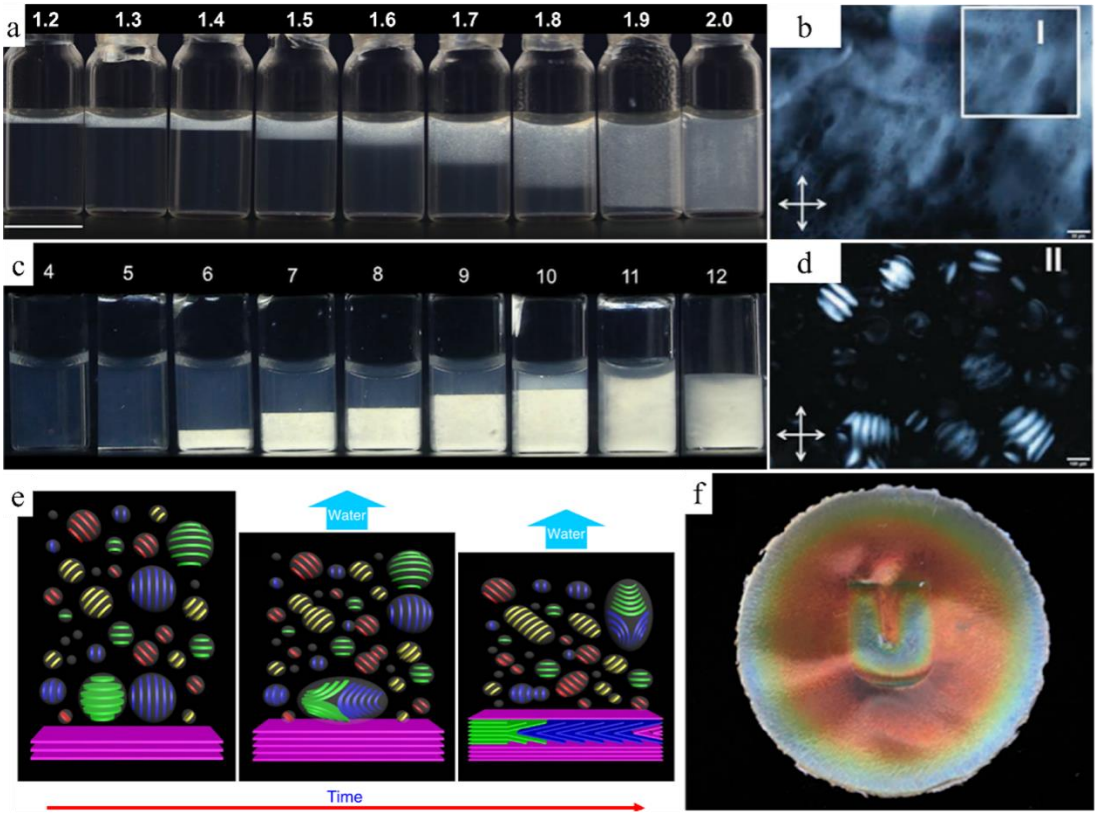

Figure 7. Colloidal suspensions after phase separation and water removal. a) Density inversion at the isotropic-anisotropic phase separation in CNC suspensions from never dried source. b) Observation of atactoids formation in the low-density LC phase. a-b) Reproduced under the terms of the CC BY 4.0 license.[91] Copyright © 2022, The Authors, published by Wiley-VCH GmbH. c) Usual phase separation in CNC suspensions with a high-density LC phase. Reproduced under the terms of the CC BY 4.0 license.[95] Copyright © 2018, The Author(s), published by Springer Nature. d) Tactoids observed in the high-density LC phase. Reproduced under the terms of the CC BY 4.0 license.[91] Copyright © 2022, The Authors, published by Wiley-VCH GmbH. e) Cartoon of a coalescence of tactoids and water evaporation that origins structural colored films. Reproduced under the terms of the CC BY 4.0 license.[86] Copyright © 2016, The Author(s), published by Springer Nature. f) CNC film patterned with cellulose acetate masks placed at the beginning of CNC suspension casting. Adapted with permission from [94]. Copyright © 2018, American Chemical Society.

Considering the range of direct applications of CNC photonic films,[82,96] they can also be used indirectly as a template for constructing novel advanced inorganic-organic composite materials, followed by the removal of CNC structure, being useful in the future for the mineralization of Bouligand structures.[97] Other applications involve the addition of small molecules or polymers in the starting suspension, which enables the control of the pitch value of the CNCs composite suspension while inducing flexibility in the final products.[98,99] Several reviews can be found where one can survey the multitude of studies done.[100,101] The system is so versatile that Qu et al. recently explored the photonic response of CNCs-based materials to external stimuli,

including electric, mechanical, magnetic, or optical triggers, in in-depth state-of-the-art revision.[102]

5. Cellulose derivatives self-assembled colored systems

Alongside cellulose nanocrystals, several cellulose derivatives self-assembly into cholesteric liquid crystalline phases. They can form thermotropic or lyotropic, or even both LC mesophases. This derivatives' LC behavior depends on the polymers' molecular weight and temperature. Still, it is primarily related to the chemical structure of the substituent, the length of the side chain of the substituent, and the degree of substitution.[103]

The earliest finding of structural coloration on a cellulosic derivative was presented by Werbowyj & Gray when a highly concentrated hydroxypropylcellulose (HPC) aqueous solution showed coloration.[104] The authors observed that the solution presented fluidity and birefringence. Later, the authors showed that the system presents right-handed cholesteric organization and self-assembly into a LC phase in other solvents.[105] In aqueous solutions, HPC forms cholesteric phases with a polymer content equal to and above 58 wt.% and presents strong colorations from red to blue if concentrations range from 60 to 66% wt., respectively, are used.[106] Please note that these data are dependent on the average molecular weight, the degree of substitution (defined as the average substitution of hydroxyl groups linked directly to the cellulose main chain), molar substitution (defined as the average substitution of all hydroxyl groups in the polymer, even branched chains) and for a specific temperature and pressure conditions.

Meanwhile, Shimamura et al.[107] demonstrated the thermotropic behavior of HPC, with a microscope coupled with hot stage and rheology studies, on a lower average molecular weight HPC. Years after, Charlet & Gray showed thermotropic behavior on HPC films solvent-casted from LC HPC/H_2O solutions.[108] The authors observed that rising the temperature of the films led to increased pitch values, although this process was not proven to be reversible. The presence of the lateral side chain plays the role of the solvent as in a lyotropic LC since it assists in the mobility of the macromolecules by incrementing the space between the polymer chains.

Several authors prepared and researched ethers and esters of cellulose, although not to the same amplitude as the cellulose nanocrystals. Revisiting all these derivatives is not the scope of this review, and information on this can be found elsewhere;[109] still, one should notice that the chemistry of the substituent, the control of the degree of substitution, and for lyotropic systems, the type of solvent and polymer content, allow tunning the pitch value of the helical structure

given by the derivative, but also its handedness; this is if the system self-assembly into a right- or left-handed cholesteric supramolecular organization.

For instance, Zugenmaier & Haurand showed that by controlling the amount of dichloroacetic acid (CH_2Cl_2COOH - DCA) in a lyotropic solution of ethyl cellulose (EC) and acetic acid (CH_3COOH - AcOH) they could change the helical handedness from left- to right-handed.[110] Previous data showed that EC dissolved in AcOH forms left-handed and when in DCA give rise to right-handed LC structures.[111] The preparation of different lyotropic solutions, where the content of DCA was increased from 0 to 100 % vol., led to the observation of the effect of the solvent on the handedness of the helical self-assembly of this lyotropic system. Indeed, the interaction of a solvent with the chiral cellulosic chain plays a pivotal function in forming the lyotropic phase by allowing its twisting into a helical structure or inhibiting it. Similar behavior was attained when ethyl cellulose was acetylated with different degrees of substitution.[112] Guo & Gray[113] were able to show that the now (acetyl)(ethyl)cellulose self-assembly into a left-handed phase with an average acetyl degree of substitution ($\overline{DS}$) of 0.06, and right-handed when $\overline{DS}$ increased to 0.5, maintaining constant the ethyl substitution ($\overline{DS}$=2.5), and the polymer concentration (50 wt.% in chloroform). **Figure 8**a shows the control of ellipticity of these lyotropic systems, also as a function of temperature between 26-42ºC, where interestingly, for the right-handed system, the increase of temperature gives rise to a redshift in the maximum wavelength, and the opposite effect is observed for the left-handed helicoidal system. This example clearly shows the importance of the chemistry of the substituents on the LC formation but also highlights the influence of the number of substituents as just a small change, as seen here, originates an inversion of the supramolecular helicoidal arrangement of the cellulosic system.

Even if the production of new cellulosic LC cholesteric systems in the last decade is not as intense as from 1980 to 2000, it is still possible to find some interesting new structures that can be promising starting materials for producing advanced functional materials. For instance, recently, Ohlendorf and Greiner prepared (methylthiopropionated)hydroxypropylcellylulose with a broader thermotropic LC phase, between -33 to 165ºC, being cholesteric above 90ºC.[114] This high range of temperature allows its introduction in several systems and composites with nanoparticles. Although the authors do not explore the handedness of the cholesteric organization, an iridescent yellow-green film can be observed in a photographic image. Ishii et al.[115] synthesized HPC with butyryl (Bu) and heptafluorobutyryl (7FBu) substituents with different $\overline{DS}$, with the condition that the sum of both $\overline{DS}$ was equal to 3. The thermotropic

system, analyzed by circular dichroism, showed to be right-handed and reflected visible light from violet to red if 7FBu $\overline{DS}$ ranges from 0.04 to 0.8. The variation of 7FBu $\overline{DS}$ allows the authors to observe an increase in pitch; however, no change in handedness was detected. The authors attributed this behavior to the decrease of the twist angle in the adjacent nematic layer, which might be related to dipolar interaction between the side 7FBu groups.

Lately, hydroxypropylcellulose has attracted pronounced attention from the scientific community since it can produce strong structural coloration in water, as discussed before, allied to its biocompatibility.

Liang et al.[116] created a colorimetric pressure sensor based on cholesteric LC aqueous solutions of HPC with polymer content ranging from 63 to 70 wt.%. Since this is an aqueous system, to overcome the problem of solvent evaporation while using these sensors, the HPC/H_2O solutions were encapsulated between polyethylene terephthalate rolls. The authors established that if working with a sensor that reflects coloration with a wavelength in the border between the near-infrared and the visible (red) regions of the electromagnetic spectrum, a blueshift in the reflected wavelength occurs when a maximum pressure of 10 kPa is applied. The larger scale of the laminated constructs and the optical response to pressure open the application of colorimetric aqueous HPC to advanced functional materials and highlight HPC/H_2O LC solutions as ideal candidates for mass production.

Using a similar principle of encapsulation HPC solution between flexible substrates, although silicone-based, Wei et al. printed hydroxypropylcellulose composite systems, where carbon nanotubes (CNT; 0.1 wt.%) and carbon nanofibers (CNF; 0.4 wt.%) were added to render conductive properties and the appropriate rheologic properties, respectively.[117] Figure 8b shows the optical response of the printed and encapsulated, with polybutylene adipate terephthalate, composite system when submitted to stretching. Panel c of the same figure shows the optical response to the temperature variation, evidencing that the presence of the CNT and CNF does not affect the LC behavior of HPC. With this new printing technique, the authors produced display demonstrators (Figure 8d) that respond to external electric stimuli, and it was possible to control each panel individually, as shown in Figure 8d2-4.

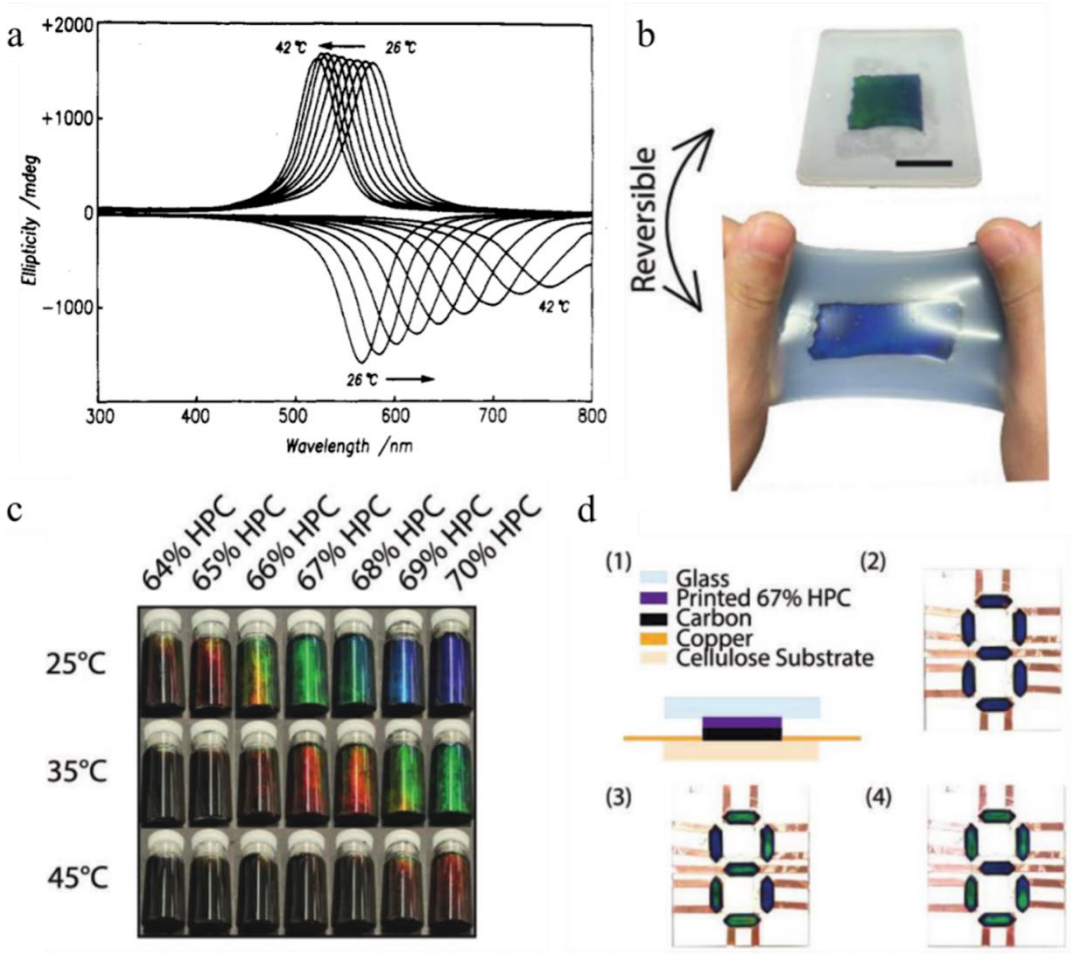

Figure 8. Colored cellulose liquid crystalline materials: a) Ellipticity of the lyotropic solution of (acetyl)(ethyl)cellulose in chloroform (50 wt.%) showing a blueshift of the maximum wavelength on the left-handed derivative, with a low degree of acetyl substitution (0.06), or a redshift of the maximum wavelength on the right-handed derivative with a higher degree of acetyl substitution (0.5) as the temperature increase. Adapted with permission from [113]. Copyright © 1989, American Chemical Society. b-d) Printed cholesteric solution of HPC in water reinforced with conductive carbon nanotubes and carbon nanofibers that give rise to b) stretchable and reversible colored changing system when encapsulated between flexible substrates (65 wt.% HPC; CNT 0.1 wt.%; CNF; 0.05 wt.% in H_2O) scale bar 2 cm, c) thermal-responsive photonic systems, d) printed electric stimuli displays as outlined in d1, showing individual response on panels d2-4. Reproduced under the terms of CC BY 4.0 license.[117] Copyright © 2022, The Authors, published by Wiley-VCH GmbH.

Balcerowski et al. explored the use of extrusion-based direct ink writing (DIW) to induce shear-orientated alignment of the cholesteric organization of HPC aqueous solutions (Figure 9a).[118] With this additive manufacturing technique, the authors intended to extend the surface area of the HPC films with fewer defects. Glutaraldehyde[119] was chosen as the crosslinking agent, and a typical small redshift on the reflected wavelength of the printed structures was observed. However, there is no angular photonic dependence when the structure is observed between 20

to 50 degrees. The authors suggested that this behavior was due to the wrinkling surface obtained in the 3D printing structures drying process observed on SEM images at different magnifications (Figure 9b).

Combining the thermotropic behavior of HPC films with structural coloration, Ming et al.[120] created microdroplets from LC aqueous solutions, starting from the same 45 wt.% HPC/H_2O solution, following emulsification with 2 wt.% of Span 80 in paraffin oil. The attained microdroplets are allowed to rest, and the appearance of cholesteric polydomains is noticeable. Different thermal treatment was applied and allowed producing microparticles that reflected blue (Figure 9c), green, and red structural coloration, owing to the helical organization retained within the solid microdroplets of HPC. Although the polydispersity of the microdroplets is very high (ranging from 50 to 550 µm), Bouligand's arc-textures are observed on SEM micrographs of a sphere cross-section revealed in Figure 9d, and at higher magnification, the helicoidal arrangement can be seen Figure 9e. With this work, the authors demonstrate that it is possible to produce edible HPC structural colored microspheres with an example of decorating a food article.

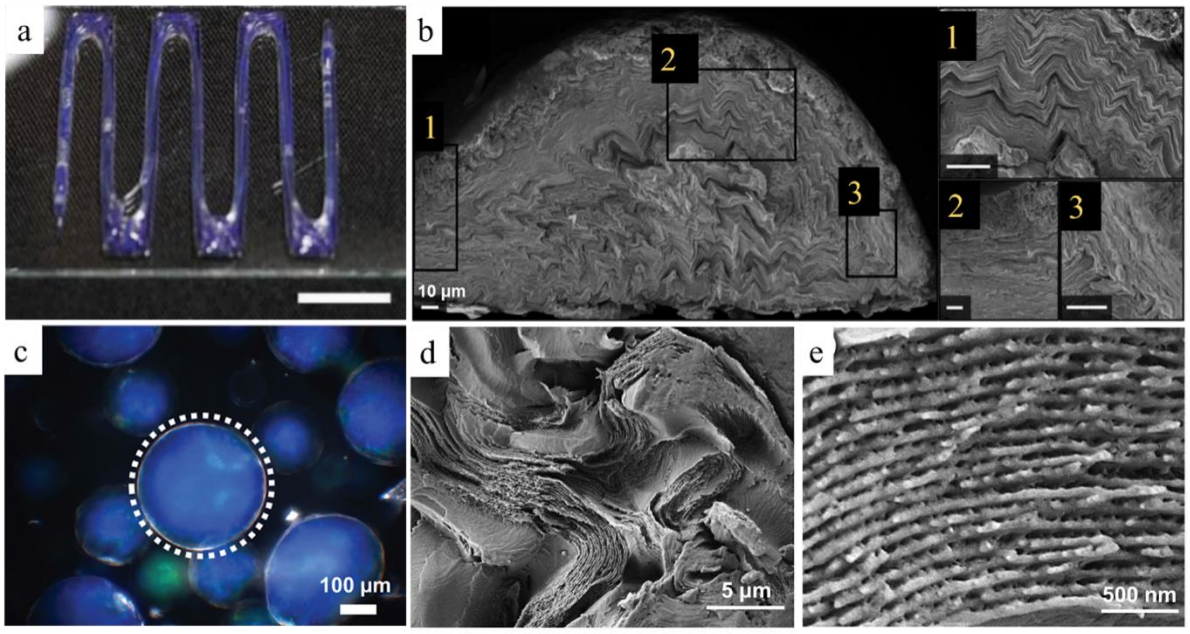

Figure 9. HPC-based 3D structures. a-b) Temperature crosslinked 3D printed structure of HPC/H_2O/glutaraldehyde LC solution where the authors notice the absence of photonic angular dependence saw between 20-50º, attributed to the wrinkled surface. Adapted under the terms of the CC BY 4.0 license.[118] Copyright © 2022, The Authors, published by Wiley-VCH GmbH. c-e) Edible microdroplets of an emulsion of LC aqueous suspension of HPC with Span 80 in parafilm oil after thermal treatment, where the strong blue structural coloration is attributed to the cholesteric organization confirmed by the presence of Bouligand arc-texture visualized by d-e) SEM images of cross-sections of dried samples. Adapted under the terms of the CC BY 4.0 license.[120] Copyright © 2023, The Authors, published by Wiley-VCH GmbH.

Chan et al. combined the thermotropic and lyotropic behavior on crosslinking a LC methacrylate-hydroxypropylcellulose solution to prepare 3D structures using extrusion printing.[121] The authors observed that after UV crosslinking and solvent evaporation, a blueshift on the maximum reflected wavelength is attained for all the range of starting concentrations studied (58-72 wt.% of polymer content), showing coloration between 62 to 70 wt.%. Structures from the same 70 wt.% HPC-MA LC solution can furthermore be crosslinked at different temperatures to attain different colored systems. After water evaporation, the films retained coloration, and the authors could blueshift the maximum reflected wavelength, contrary to the usual redshift observed for HPC-MA films when subjected to an increase in temperature (from 22 to 30 ºC). In order to do so, the authors increased the environmental humidity during the crosslinking step, inhibiting drying. **Figure 10**a shows a schematic representation of the 3D printing systems with a UV source, where the model of the alignment of the cholesteric domains along the extrusion process suggested by the authors is shown, implying that radial aligned cholesteric domains are achieved when the filament is extruded. Figure 10b exhibits a 3D gecko of HPM-MA from LC HMP-MA aqueous solution, and Figure 10c presents 3D printed HPC letters with different structural colorations, produced from the same starting solution, obtained at different crosslinking temperatures.

Using the ability that HPC has to self-assemble into a LC phase in water was also explored by Zhang et al., to produce 3D objects non-iridescent that respond to temperature as an external stimulus.[122] In this system, the authors combined the LC nature of aqueous HPC with gelatin, which allows rheologic tunning, and poly(acrylamide-co-acrylic acid) pre-gel, which allows photo-crosslinking in the printing process. From rheology, the authors determined that this ink is printable at high shear rates and, at low shear rates, relaxes into a gel-gaining structure. The authors were able to produce with the same system multicolored structures in a diversity of shapes with good reproducibility and demonstrate that the same construct can change from green to orange when a temperature change of 20 ºC was induced.

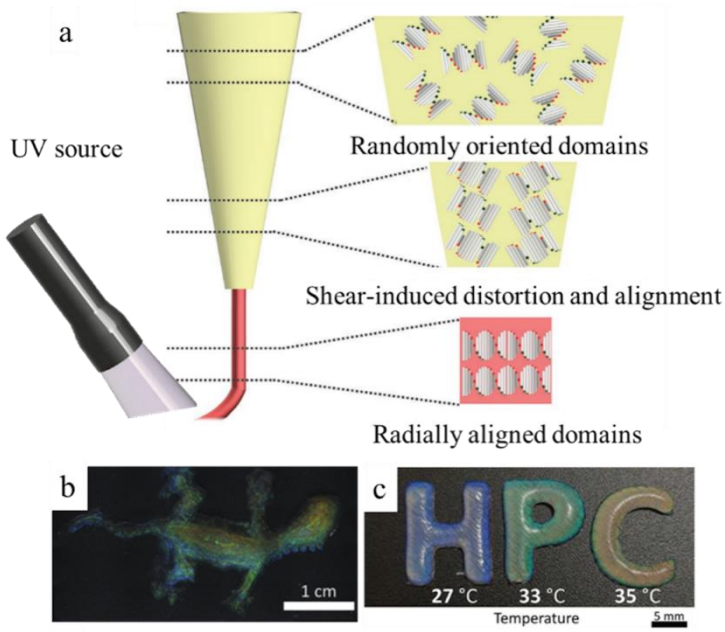

Figure 10. Colored Tunable HPC-based 3D printed structures. a) Schematic representation of the alignment of cholesteric domains on the production of 3D structures by extrusion method from a LC solution of HPC-MA crosslinking with UV light followed by drying at different temperatures, b) printed gecko and c) H, P, C lettering dried at different temperature starting from the same HPC solution. Adapted under the terms of the CC BY 4.0 license.[121] Copyright © 2022, The Authors, published by Wiley-VHC GmbH.

More recently, and similar to the research done with CNCs, some works can be found where compatible polymers are added to HPC solution to induce a kinetic arrest of the pitch at a specific value. George et al. use polyethylene glycol, with low molecular weight (200 $g.mol^{-1}$), in 3D printed structures of HPC/PEG, and the authors were able to establish a set of parameters that can be useful to obtain tailormade constructs.[123] If printed at low shear rates, this new ink results in well-organized nanostructures with almost no angular color dependence. If, on the contrary, printing occurs at high shear rates, the authors estimated that a preferred alignment of the cholesteric pitch along the printing path with an angle of 20º occurred. The presence of PEG allows the system to retain structural coloration in the visible range when the solvent was removed at lower temperatures (for example, reducing 20 ºC in the drying process) in a postprocessing step.

Although these noteworthy results with HPC LC solutions shed light on using photonic cellulose derivatives in additive manufacture and mass production materials, the handedness of the cholesteric organization of such is not discussed. However, from previous works, it is known that HPC aqueous solutions self-assemble into right-handed helicoidal structures, so the increase in volume observed in these 3D printed systems is not expected to give an inversion in handedness.

6. Cellulose self-assembled out-of-equilibrium systems

If instead of water, organic solvents, weaker acids, or stronger acids are used to dissolve a cellulose derivative, a liquid crystalline phase may also be formed, as seen with cellulose acetate dissolved in trifluoracetic acid (TFA - CF_3CO_2H). Indeed, Ritcey et al. observed a rapid esterification reaction, where the free hydroxyl groups of the derivative were substituted by trifluoracetate groups [124], releasing water molecules. The left-handed liquid crystalline structure evolved with time, increasing the maximum reflection wavelength after some hours. After some days, a handedness inversion of the helicoidal structure from left- to right-handed was detected. During the timescale of the experiment, no degradation was observed. In the cellulose acetate system, the TFA had two roles: it served as the solvent that led to forming a liquid crystalline phase and acted as a reactant via an esterification reaction.

Hydroxypropylmethylcellulose (HPMC), or Hypromellose, is a derivative highly used in the pharmaceutical industry, but also in the food segment, mainly due to its gelation properties, allied to biocompatibility and solubility in water, among other solvents. It forms liquid crystalline solutions in TFA and as cellulose acetate, the free hydroxyl groups can undergo an esterification reaction and be replaced by trifluoracetic ones (**Figure 11**a). This LC system was recently revisited, and the striking evolution of structural coloration was followed with time (Figure 11b, c) where a food grade HPMC, with low molecular weight, dissolved in TFA was placed inside a capillary structure (optical path of 0.40 mm).[125] If the capillary was closed or open, an unexpected evolution of sequenced structural coloration was observed with time (Figure 11b-c and d, respectively). These color sequences resemble the sequences encountered on the concentric rings of structural colors detected on drop-casted films attained from aqueous LC suspensions of CNCs. In these CNCs films this fact is attributed to the uneven capillary flow alongside the droplet[126] as the solvent evaporates and nanoparticles are pulled to the periphery of the film. Nevertheless, this explanation does not justify what the authors observed for the confined HPMC/TFA LC evolutive system, and 1D molecular diffusion reactions, alongside the esterification reaction, were proposed. Figure 11b shows a sealed capillary one hour after preparation, and the microscopic observation, in reflection mode, of the different colored sections. After 2 days, the same capillary shows different colored domains (Figure 11c). According to the authors, the diffusion of TFA from the center of the capillary to the periphery as time passes happens, taking the system to an out-of-equilibrium state, where this phase is now rich in the solvent, and the pitch of the LC phase around it increases. Contrarily, the next

area of the capillary presents a higher content of polymer (product of esterification reaction), and the pitch value of this section is reduced. So, the pitch changes from red to green to blue if one looks at the bottom of the capillary, and in the next section, it undergoes a similar process originating a color sequence of blue-green-red. It is worth mentioning that while the esterification reaction happens, a molecule of water is released per hydroxyl group substituted, and this molecule is also involved in the set of diffusion reactions, as not only TFA but also water is diffused alongside the sample.

In Nature, one can find similar gradient-colored patterns as peacock feathers or beetle *Pachyrrhynchus congestus pavonius* spots. Although the structural coloration on this last animal is not attributed to the twisted structures but to 3D photonic crystals,[127] the appearance of these eyespots is remarkable. On the other hand, color pigmentation seen on the eyespots on peacock feathers was attributed to reaction-diffusion models[128] as in the HPMC/TFA LC system proposed above.

The reaction-diffusion model for HMPC/TFA was further investigated by Silva et al. in a quasi-2D construct (with 65 μm) where a droplet of HPMC/TFA in a LC mesophase was placed between two glass substrates.[129] At room temperature, the now open sample pocket allows the solvents, TFA and H_2O, to diffuse and evaporate from the center of the droplet to the meniscus. As the hours passed, this phenomenon originated differences in the structural colorations from those observed from the 1D preparations. If observation of the structural color is followed in time, as seen in the photographs of Figure 11d, the bright left-handed structural colors start only to be intense at the center of the droplet, while at the edge of the droplet, a white color advances. This evolution is followed by a faint right-handed circularly polarized light reflection (Figure 11d), where a pale blue coloration appeared around the time of 60 hours. Pitch value determination, with microscopy in transmission mode with cross polarizers (Figure 11e), allows the authors to see an increase of the pitch value from the center of the droplet, passing to a zone with no pitch value, attributed to a nematic regime, and following a region with a decrease in the pitch value as we travel to the outer zone of the droplet. With the application of the reaction-diffusion model and evaporation of the solvents at the boundaries, simulation of the spatio-temporal evolutive variation of the structural coloration observed experimentally on the droplets of the HPMC/TFA in these quasi-2D preparations was achieved. Solid films were obtained from each stage; this is when LCP or RCP light reflection was observed, which allows for obtaining hydrophobic or hydrophilic surfaces on demand. The out-of-equilibrium systems pave the way for using dynamic systems as time-evolution stamps or time-controlling tags.

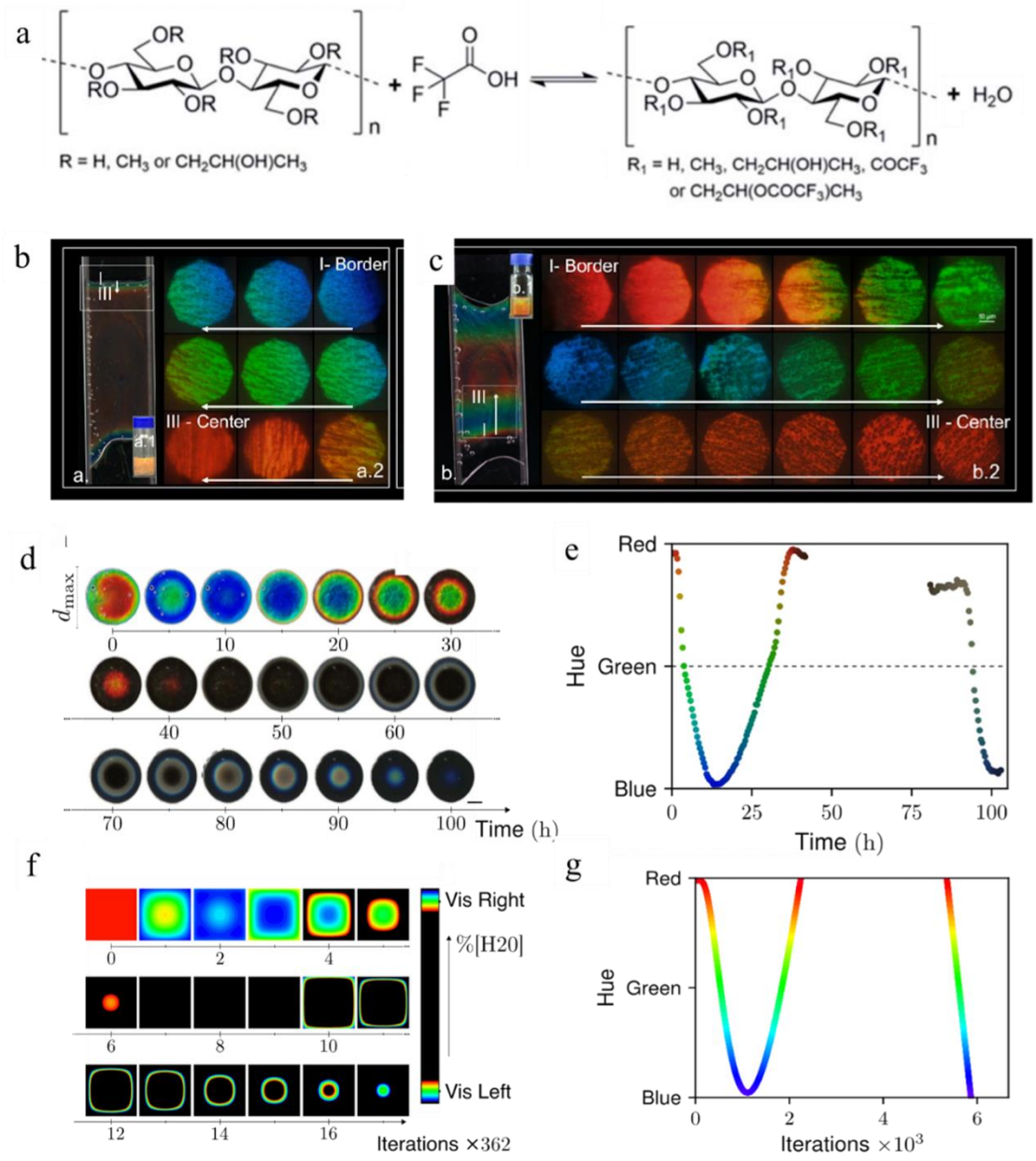

Figure 11. Out-of-equilibrium cellulosic systems with time-evolving coloration. a) The chemical reaction involving the cellulose derivative and the carboxylic acid. Observation of the sequenced structural coloration on a 1D preparation of HPMC/TFA LC solution after b) 1h of preparation and c) 2 days after preparation followed by POM on reflection mode between cross-polars. b-c) Reproduced from [125] with permission from the Royal Society of Chemistry. d) Photographs of the evolution of structural coloration with time of a droplet of HPMC/TFA LC on a quasi-2D geometry, where b) shows the sequential appearance and the reappearance of color in d. f) Numerical simulation showing the spatio-temporal evolutive color variation based on the reaction-diffusion model and evaporation of solvents from the boundaries, with the corresponding e) evolution of color on the center of the square. Reproduced under the terms of the CC BY 4.0 license.[129] Copyright © 2021, The Author(s), published by Springer Nature.

Ackroyd et al. used reaction-diffusion systems to organize a composite system of nanoparticles[130] rather than macromolecules as the system described above. The authors

observed the formation of the films as water evaporates from droplets of a suspension of cellulose nanocrystals (CNCs) with L-(+)-tartaric acid (TA) deposit on a glass surface, on chambers with different relative humidity, **Figure 12**a (ratio TA/CNC: 0-9). As the solvent evaporates, saturation occurs, leading to local phase separation of the two components, followed by precipitation and nucleation reactions. The process is repeated; this is phase separation, followed by precipitation and diffusion leading to rings either rich in CNCs or TA, creating a ringed pattern, as can be seen in the images of Figure 12a. The periodicity, here expressed by the letter P (μm), is controlled by the TA content on the mixture (Figure 12b) and relative humidity imposed in the evaporation process. The proposed reaction-diffusion mechanism, applied in a numerical simulation, fits the experimental results. This new methodology allows producing new functional materials, where the precise control of separation of two components in these rings can be controlled on demand, where a cholesteric organization (Figure 12c) parallel to the plane of the film is retained in a CNCs solid section, followed by elongated tartaric bundles aligned in a radial direction Figure 12d.

The out-of-equilibrium systems and their application to produce materials capable of being employed by the end user seem to be gaining some interest within the scientific community. Although in its early stages, this fosters the development of an edible colorful HPC/shellac timer. In this new system, dry HPC films, derived from a cholesteric HPC solution, were encapsulated between water-permeable shellac coatings. The authors examined the color evolution with time and observed the difference between the evaporation and hydration process, where 12 h were sufficient to induce a system with light reflection lower than the wavelength of Vis light (Figure 12e and g). However, it took more than 24 h to rehydrate the system if starting from a dryer state (Figure 12f and g). This disparity in time was attributed to the difference in the diffusion dynamics of water within this these two stages, being slower if starting from a dehydrated state. These interesting preliminary results also showed that the authors could control the colored time dynamics by adjusting the thickness of the coating.

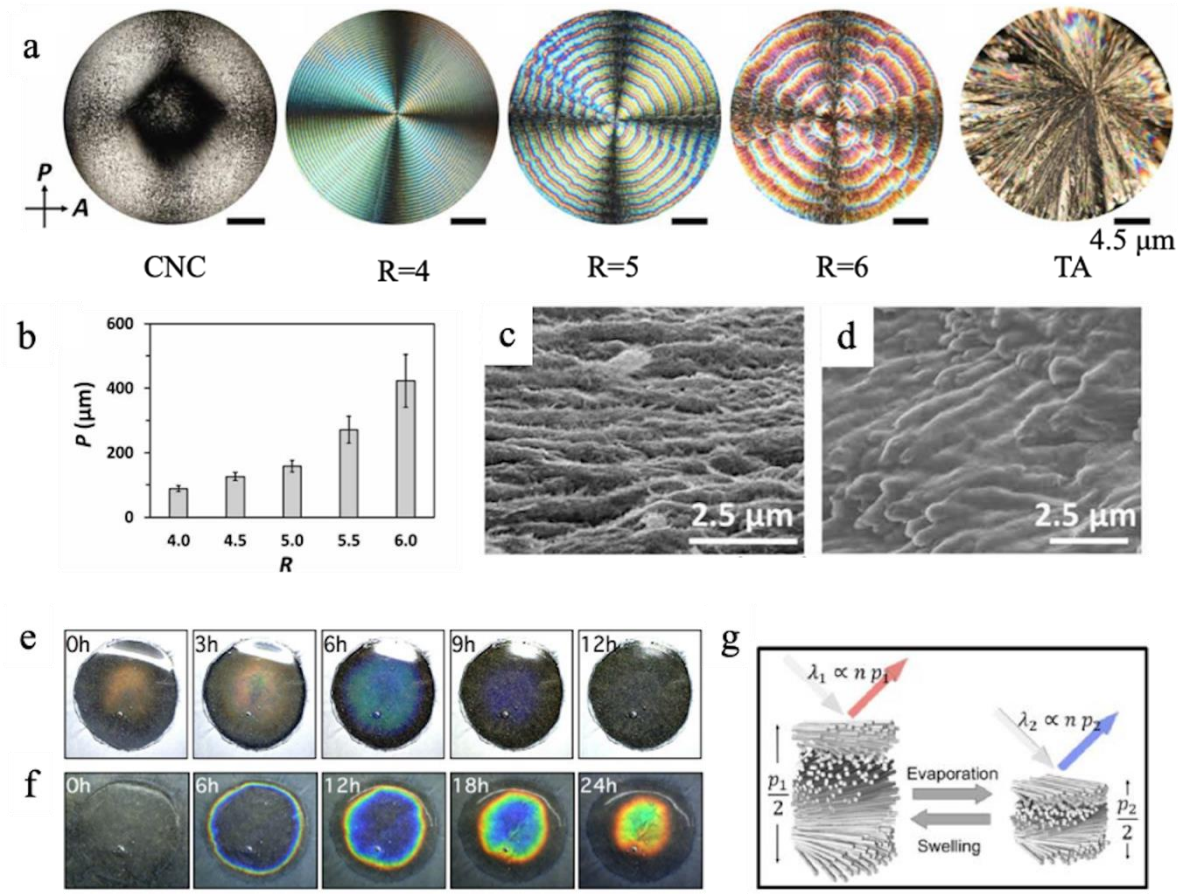

Figure 12. Out-of-equilibrium of CNC and HPC-based systems a) POM images of CNC, CNC/tartaric acid, and tartaric acid films (from left to right), observed with cross-polars, where R represents the ratio between TA/CNC. The concentric colorful rings were attributed to diffusion reactions, where enrichment of a specific material is seen, giving rise to films with separated phases of CNC/TA/CNC/TA, b) where the R allows modulation of the periodicity of the rings. Differences in the morphology of the enriched phase of CNC c) and TA d) on a film with R=4.5 can be seen in the SEM images. From [130]. Copyright © 2021, The Authors, some rights reserved; exclusive licensee AAAS. Distributed under a CC BY-NC 4.0 license. Adapted with permission from AAAS. Colorful 2D system of cholesteric HPC film encapsulated in water-permeable shellac coatings, where color evolution can be seen in a e) drying process and f) re-hydration process. g) Schematic representation of the pitch difference during evaporation/swelling process, attributed to water diffusion dynamics within the construct. Reproduced under the terms of the CC BY 3.0 license.[131] Copyright © 2023, The Authors, published by The Royal Society of Chemistry.

7. Chitin-made structures

7.1. Helicoidal structures *in vivo*

7.1.1. Optical properties

The twisted plywood hierarchical structure (**Figure 13**a) is a ubiquitous motif across the Arthropoda phylum. This structure can be part of the animals' optical devices, which evolved in the Cambrian period, and the earliest reflector acknowledged dates circa 508 million years

ago (Ma). The eyes with lenses probably developed at about 521 Ma when the introduction of vision led to the so-called Cambrian explosion. Until this time, all animals had soft bodies and were mostly worm-like.[132–135] Records from fossil specimens of beetles aged 15–47 Ma demonstrate reflection colors,[136] as can be seen in Figure 13b.

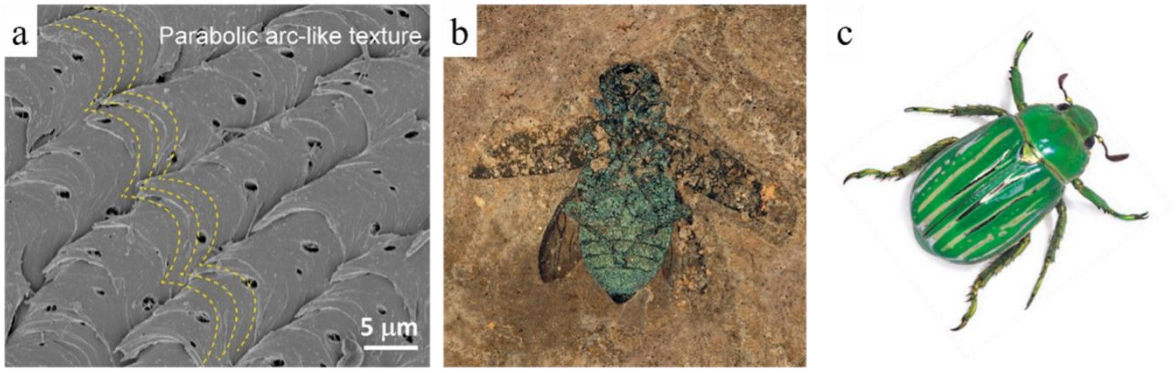

Figure 13. Chitin self-assembled natural systems: a) SEM cross-sectional image showing the arc-like texture in the exocuticle of the horseshoe crab *Tachypleus tridentatus*. Adapted from ref. [137], Copyright © 2022, with permission from Elsevier Ltd. b) Fossil jewel beetle found in the Messel pit (Germany). (T. Wappler, Hessisches Landesmuseum Darmstadt, Germany. CC BY-SA 3.0).[138] c) *Chrysina gloriosa.* (P. Beckmann. Copyrighted free use).[139]

Light can act in animal evolution by explaining the diversity of natural photonic structures.[140] Color and polarization in the living world influence the chance to survive and reproduce.[141,142] In fact, animals may use their colors for sexual communication,[143,144] for cryptic behavior,[145–147] and for warning predators.[148] Thin-film and multilayer interference, photonic crystals, diffraction grating effects, or light scattering are responsible for most structural colors. Animals have evolved designs to achieve, at the same time, light scattering in wide-angle values and high reflectivity in a given wavelength scale. Both criteria appear to contradict one another, yet both needs are met by integrating the structure's regularity and irregularity.[149]

It is challenging to replicate the natural structures due to the complexity of the fascinating biological designs. Often, numerical optimization is used in photonics to predict optical structures toward on-demand complexity and energy consumption inspired by natural evolution.[150] The evolutionary perspective might help us to understand how evolutionary pressures led to the adaptation of material structure.[151] Besides numerical optimization, the commonest stereotypical natural photonic structures were retrieved through the use of evolutionary algorithms. For that, specific optimization methods were used, such as maximizing reflection for a certain wavelength, for an extensive array of wavelengths, or maximizing the dispersion of light. The evolutionary algorithms support the sense that evolution is a successful

optimization path by exhibiting that distinctive natural-based photonic structures are the best solutions to significant societal issues.[152]

The Coleoptera order, belonging to the Arthropoda phylum, comprises ca. 400 000 species, several exhibiting interesting optical properties, such as iridescence, narrowband and broadband metallic colors, brilliant whiteness, and distinct polarization signatures.[153–155] In nature, circular polarization is not a commonly observed optical effect, contrasting with linear polarization. When CP light interacts with the beetles' cuticle, left-handed circular polarized light, at normal incidence, is reflected. An exception to this phenomenon is observed on the jewel scarab *Chrysina resplendens*,[156] which exhibits a cuticle with a specific construction consisting of two spatially distinct left-handed cholesteric layers separated by an anisotropic domain; This latter, for which the fibers are parallel, performs the function of a half-wave phase retarder, leading to the cuticle's reflection of both LCP and RCP waves.[157] Biomimetics of the three-layer system has been elaborated using polymers[158] and CNCs.[159,160] These works aim to create both-handed circularly polarized reflectors with large reflected light fluxes, exceeding the 50% limit of a CLC structure with a single helicity sense and polarization-independent reflectors.[161]

The investigation of the optical and structural characteristics of scarab beetles' cuticles has been concentrated on a relatively small number of cases. However, one can find repeated descriptions of identical structures.[153] Several works can be found where the authors analyzed the genus *Chrysina*, often known as "jewel scarabs" due to their vibrant light reflection properties, ranging from bright green to metallic silver-gold, *i.e.,* giving rising to selective or broadband reflection.[162–165] Within this *genus,* the tessellated *Chrysina gloriosa* cuticle draws attention because of its alternating silver and green bands (Figure 13c). Due to its complex photonic structure, the cuticle of *C. gloriosa* shows, in a single and unique layer, extreme cases of obliquity of the orientation of the helical axis.[166] Its entire cuticle reflects LCP light. The silver bands are not patterned and behave as specular broadband mirrors.[167] The green bands have a polygonal texture (insert in **Figure 14**a). TEM cross-sectional views reveal a pitch gradient from the visible to the infrared spectrum (Figure 14a). The fingerprint (striped) texture then progresses from the exocuticle (top part) to the endocuticule (lowest part). The undulations of stripes in the exocuticle below the polygons indicate that the helicoidal axis is not constant in space. Parallel stripes in the endocuticle are seen because these variances diminish in depth. The texture in the endocuticle appears to be less uniform (stripes are disrupted) and grainy, as seen in the *Homarus americanus* exoskeleton.[168] It is thought that the existence of a cholesteric

grating with a bigger pitch in this section of the beetle's cuticle might prevent overheating. Polygons, with a mean size of 5 μm, behave like micromirrors with a reflection pattern (donut or spot) that varies with incident wavelength.[167] With a spectral resolution of 6 nm and a spatial resolution of 150 nm, the hyperspectral imaging approach relates the topography of iridescent polygons to the complex twisted structure (Figure 14b).[166] Hyperspectral datacubes show the spatially resolved spectral reflectance in two cube sides (wavelength *vs*. each dimension of the surface of the band) and the average reflectivity on the top of the cube (surface of the band). The topographic data incorporates the geometrical variations (relief) and the internal twist distribution in the exocuticle and endocuticle. It exposes similarities and variations in the spectral-spatial characteristics of biological and synthetic samples, which are currently designed.[169] Phase measurements provide evidence that the preservation of helicity in light reflection coincides with changes in the dynamic phase linked to the length of the optical path. This manipulation of light distinguishes itself from the characteristics of materials sensitive to polarization, which shape light by modifying the geometric phase resulting from polarization transformations. Polygons act as axicon cells generating Bessels beams with subwavelength spot size[170] (Figure 14c). Bessel beams are non-diffractive beams; they offer some diffraction resistance and may be used instead of Gaussian beams. Applications of these systems can envisage optical trapping, long-distance self-healing beams, sharp focusing, or encryption in optical communication.[171] The colors of the Bessel beams may change with the distance from the cuticle (Figure 14d). In polarization-sensitive light-shaping technology, potential bio-inspired applications arise by integrating polarization-selective reflection and multibeam interference. These applications offer spatial light modulation without the need for metasurface design. A circularly polarized light-emitting random laser was fabricated on the surface of the cuticle of *C. gloriosa*.[172] The angular distribution of the random laser emission under various pump illumination conditions was analyzed, and both left- and right-handed circularly polarized light was emitted at different angles. The work presented before demonstrates potential applications that include the development of 3D holography.[173] Another example that can be used in optical cryptography is a high-fidelity biomimetic design of the *C. gloriosa* cuticle, developed by Scarangella et al..[174]

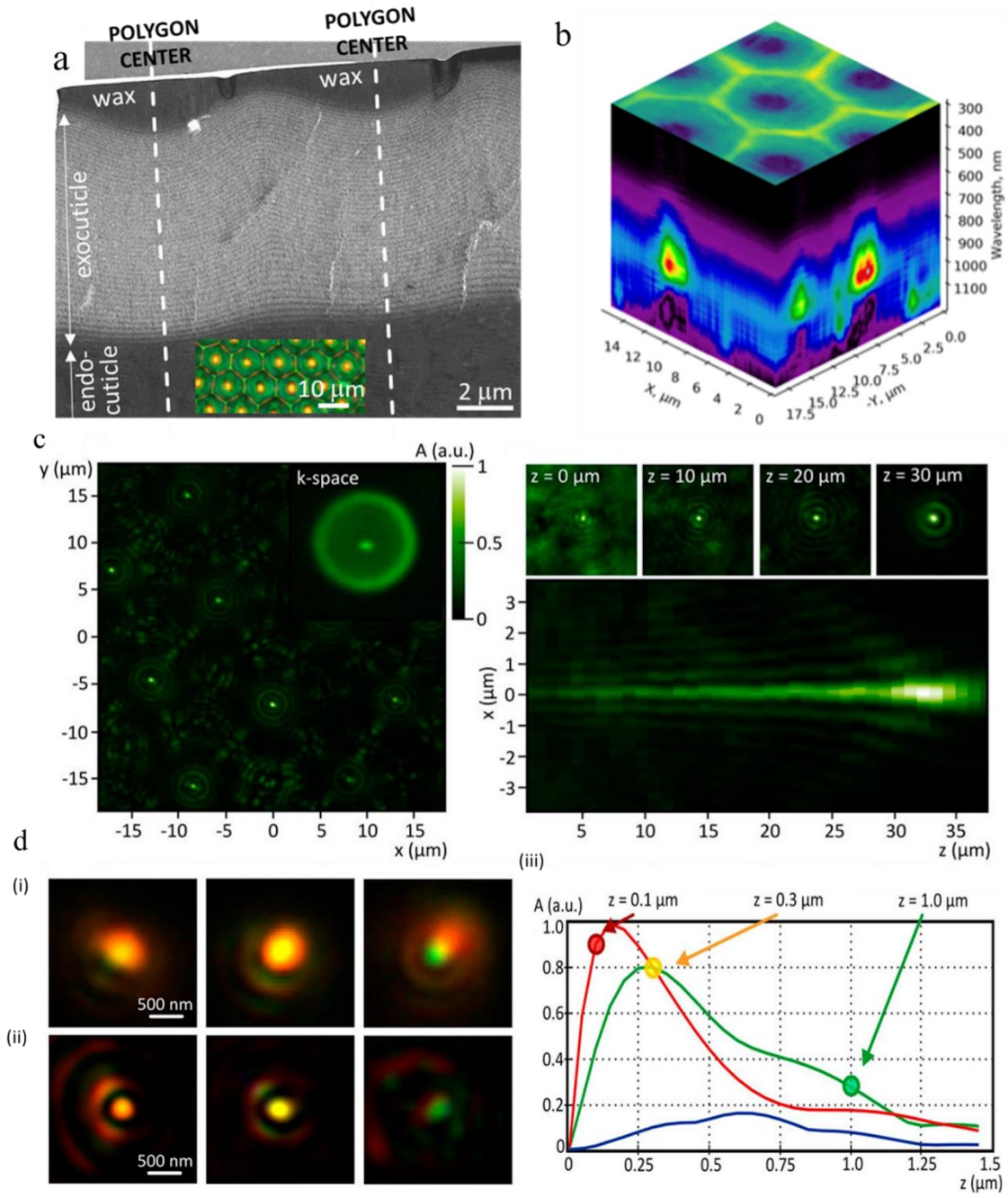

Figure 14. Characteristics of self-assembled chitin structures: a) TEM cross-sectional image showing the pitch gradient in the fingerprint texture in the scarab beetle *Chrysina gloriosa* cuticle. Insert: Optical micrograph of the polygonal texture in the plane of the green bands. Adapted from ref. [169]. Copyright © 2020, The Author(s), published by the Royal Society. b) Hyperspectral datacube of the green band. The black-to-yellow color bar indicates the overall reflected intensity (i.e., not spectrally resolved), as plotted on the top of the cube (Y vs. X). The second color bar (black-to-red) indicates the reflected spectral intensity, plotted on the cube sides (wavelength vs. X, wavelength vs. Y). Adapted under the terms of the CC BY license.[166]. Copyright © 2020, Author(s), published by AIP Publishing. c) Optical imaging of Bessel beams generated by axicon cells of *C. gloriosa*. Left: Array of Bessel beams created by individual cells and the spatial spectrum measured in k-space (optical Fourier transform of the beam array). Right: Cross-section of the propagating Bessel beam and its spots at different distances. Adapted under the terms of the CC BY license. [170] Copyright © 2019, Author(s), published by

AIP Publishing. d) Colors of the Bessel beam shaped by *C. gloriosa* at different distances from the cuticle. (i): Color image spots obtained by optical measurements. (ii): Color image spots numerically reconstructed from a single axicon cell's measured amplitude and phase (iii): Change in the weighted axial intensity of the R, G, and B colors of the numerically reconstructed Bessel beams as a function of the distance from the cuticle. Adapted under the terms of the CC BY license.[170] Copyright © 2019, Author(s), published by AIP Publishing.

Chalcothea smaragdina's cuticle contains a blazed grating that modifies the diffuse appearance of the reflected color, improving the angle-independence of the chafer's green hue and camouflage.[175]

It should also be noted that nature contains examples of cuticles that do not have a twisted plywood structure. For instance, the cuticle of the scarab beetle *Cyphochilus* is made of a network of filaments aligned parallel to the surface.[176] As such, the light scattering is increased perpendicularly to the cuticle surface, resulting in high brightness and a reflectance of 70% over the visible spectrum.

The exoskeletons of many crustaceans are not iridescent due to insufficient order in fibers' organization.[177,178] Despite the dull appearance of the king crabs' outer shells, slightly iridescent colors may appear inside their exoskeletons.[179] The endocuticle exhibits a twisted configuration with a higher structural organization than the exocuticle. Nonetheless, the arrangement of fibers gradually loses its orderliness from the inner to the outer regions of the exoskeleton, similar to the findings documented by Bouligand.[20]

The pitch tunability enables adjustment of the Bragg band (mean wavelength, bandwidth, and bandgap shape). Because the direction of the twist axis is not constant in the plane of the cuticle, the presence of tessellations in the carapace (like in the two-band cuticle of *C. gloriosa*) allows tuning of Bragg band features and the nature of the polarization of the reflected light at oblique incidence. These two features almost allow the tuning for a wide range of parameters without changing the composition.

The similarity in the geometric arrangement of helicoidal fibers within extracellular matrices has given rise to the hypothesis that they might be formed through a precursor liquid crystalline phase rather than directly controlled by cells. In the tibia of the migratory locust *Locusta migratoria* (**Figure 15**a), sets of fibers with unidirectional and helicoidal arrangements occur during daily growth.[180] A helicoidal arrangement is formed at night, whereas a parallel one is produced during the day (Figure 15b). The cellular control directly dictates the orientation of the fibers in the unidirectional arrangement. On the other hand, the helicoidal structure is formed through self-assembly away from the cell surface. The utilization of focused ion beam/scanning electron microscopy (FIB/SEM) and scanning X-ray scattering reveals that the initial fiber

orientation in the locust cuticle is determined by the epidermal cells. The ultimate architectural formation occurs through the self-organized co-assembly of chitin and proteins. Hence, the fiber orientation in the locust cuticle is influenced by both active and passive mechanisms.

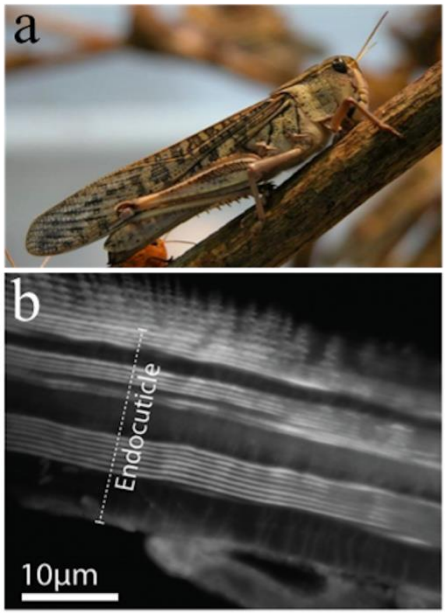

Figure 15. Twisted chitin structure. a) *Locusta migratoria*, or migratory locust. (J. Hornung. CC BY-SA 2.0 DE).[181] b) Confocal light scanning microscopy image of a stained tibia cross-section showing daily fiber growth in unidirectional and helicoidal fiber organizations, resulting in non-striped and striped textures that alternate. Adapted under the terms of CC BY license.[180] Copyright © 2020, American Chemical Society.

Protein and polysaccharide-based materials are made by nature for reuse. For all elements in a given organism, it is preferable to have functionality brought via a unique structure rather than secreting a novel material. Nature's strategy consists of a material lifetime tailored to the purpose, followed by degradation and reuse.

7.1.2. Mechanical strength properties.

The mechanical properties of the American lobster's cuticle make it a perfect material for studying.[17] Due to the twisted plywood arrangement of the fibers, the stiffness of the in-plane direction is greater compared to the normal direction. By incorporating both twisted plywood and honeycomb structures, the material achieves improved mechanical properties, reducing weight and optimal utilization of materials. This design also contributes to energy savings for the organism. The fibers are incorporated into the protein matrix and stabilized in a way that resembles steel-reinforced concrete constructions.[182] Because fibers rotate parallel to the

cuticle's plane, either gradually or abruptly, complex helicoidal designs and related textures (arc patterns) emerge, which depend on the degree of rotational displacement.

The connection between the structure and damage tolerance of hammer-like dactyl clubs found in stomatopods, a group of crustaceans, was made.[183] They are well-known for their ability to break shells using quick and forceful strikes of their appendages. *Odontodactylus scyllarus*, belonging to the stomatopod order, exhibits a composite structure comprising an oriented arrangement of crystalline hydroxyapatite and amorphous calcium phosphate and carbonate alongside a helicoidal arrangement of the fibrillary matrix. The pitch-graded architecture of such composite is responsible for dissipating the energy released by propagating micro-cracks. The twisted plywood structure is proven to make a significant contribution in preventing cracks from propagating.[184–186] Due to the inability to propagate along a linear path, the crack's trajectory enhances energy dissipation and increases impact resistance.

7.2. Twisted structures *ex vivo*

The insect exuvial dry mass is composed of a chitin content of up to 40%, depending on the species.[187] Fungal chitin would be an alternative to animal chitin.[188] Finding strategies to obtain biomimetic twisted structures is challenging due to chitin's insolubility in aqueous media[189] and the difficulties in maintaining the fibers twisting during processing.[190] The solubility depends on the crystal allomorph and the degree of surface acetylation.[191,192]

Methods were developed based on self-assembly features and colloidal suspension structures as templates to get materials combining the twisted plywood structure, the iridescence, and the mesoporosity.[193] Transferring chitin chirality into photonic porous materials offers potential applications in photonic sensors,[194] electrochemical biosensors with chiral recognition,[195] and enantioselective adsorption.[196] Iridescent membranes are obtained after purification of the cuticle removed from the inside shells of king crabs.[179] Furthermore, the mesoporosity of cuticle membranes results from mineral and protein removal from the interstices between fibers during this treatment. Cuticles formed by twisted chitin and calcite composites inspire the production of templates and scaffolds for bioceramic materials with enhanced mechanical properties.[197,198] They may exhibit a tensile strength of about 22 MPa, which is above the mechanical strength of liquid crystalline chitin-assembled films (about 10 MPa).[199]

Although some advanced materials are produced from chitin, this naturally occurring polymer is mainly used in its deacetylated form, known as chitosan, which shows solubility and processability properties in acidic conditions.[200] Chitosan can be produced by treating chitin

with enzymes or alkaline solution at high temperatures.[201,202] It is more functionally adaptable than chitin.[203] Potential applications of mesoporous chitosan structures with a twisted plywood structure address the energy storage,[204] the optical sensing,[199] the chiral separation,[196] or load-bearing functions (**Figure 16**).[205] Nonetheless, because of its low crystallinity and high gelation qualities, lyotropic liquid crystalline chitosan is challenging to obtain, and the amount of waste generated during chitosan manufacturing can be seen as a barrier to long-term use.[206] Hence, the focus of this section has been on liquid crystalline formations based on chitin.[207]

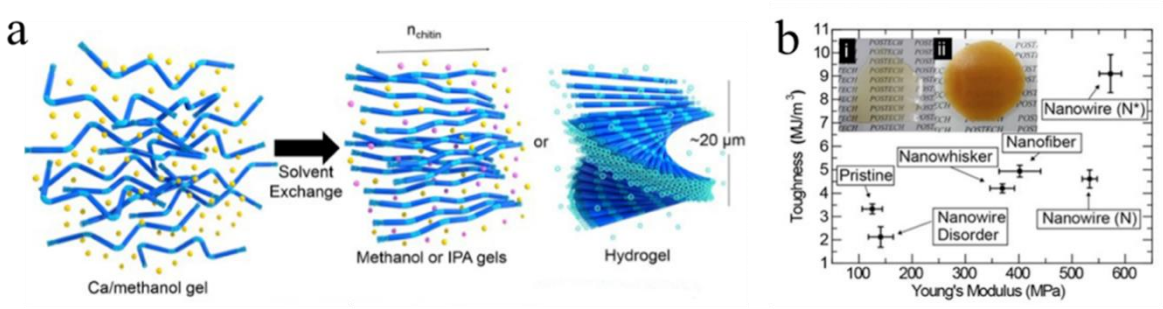

Figure 16. Chitin helicoidal hydrogels: a) From pure chitin to a twisted hydrogel. Calcium-saturated methanol disintegrates chitin fibers generating a Ca–methanol gel (left). Ca^{2+} ions are removed by washing with alcohol and deionized water, thus generating alcohol gels with a nematic N (middle) or a hydrogel with a twisted structure N^* (right) structure. The yellow, pink, and blue beads represent three different types of solvent molecules: methanol-solvated Ca^{2+}, alcohol and water. b) Mechanical reinforcement of twisted nanowires to epoxy resin. Young's modulus and toughness of pristine epoxy and chitin–epoxy composites. The inset pictures (i) and (ii) show epoxy and composites, respectively. Both Young's modulus and toughness increase as the higher-ordered structures are formed. N: (achiral) nematic structure, N*: twisted structure. Adapted under terms of the CC BY 4.0 license.[205] Copyright © 2016, The Author(s), published by Springer Nature.

The difficulties in producing cholesteric chitinous materials with structure control resulting in iridescence are described in reference [193]. Carefully controlling the acid hydrolysis conditions and post-treatment steps yields significant results in the self-assembly behavior of ChNC suspensions.[208,209] Some parameters can be controlled during the chitin extraction process, such as the hydrolysis time and acidity, directly affecting the degree of acetylation, for example. The effect of ionic strength, pH, and tip sonication energy also influences the tuning of the liquid crystalline behavior (**Figure 17**a). The helicoidal ordering can be stored in dry films by controlling water evaporation. The pitch can also be tuned in the infrared spectrum by varying the HCl and NaCl concentrations in the chitin suspension.[209] Even if all experimental parameters are controlled, the resultant films are transparent in the visible light range. The experimental difficulty in achieving sub-micrometer pitches and the intrinsically poor birefringence of chitin hampered film coloring. Some authors claim that an *in situ* alkaline

treatment can boost birefringence[210] (Figure 17b). This technique was combined with careful control over the formulation of ChNCs suspension to create structurally colored films with tunable reflectance from blue to near-infrared. When compared to shrimp ChNCs, the mesophase behavior allowed access to substantially smaller pitches in solid films.

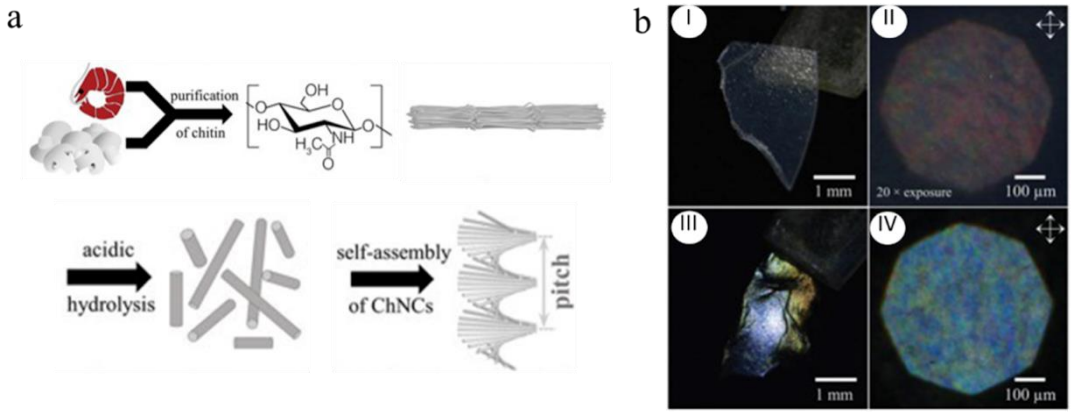

Figure 17. Optical characteristics of chitin helicoidal structures: a) A schematic illustrating the extraction, formation, and self-assembly of ChNCs. (Adapted under the terms of the CC BY 4.0 license.[210] Copyright © 2022, The Authors, published by Wiley-VCH GmbH). b) Enhancing structural coloration by alkaline post-treatment of ChNC films. I: Optical micrograph of an apparently colorless flake from a fungi ChNC film. II: The flake in I by using crossed linear polarizers. Increasing the exposure reveals the presence of weak red and green colorations. III: A flake after alkaline treatment, exhibiting strong blue and green colorations. IV: The flake in III, confirms higher reflectance and a blueshift of the reflected color. Adapted under the terms of the CC BY 4.0 license.[210] Copyright © 2022, The Authors, published by Wiley-VCH GmbH.

Deacetylated chitin membranes (DCMs) obtained from cuticle membranes of king crabs used as biotemplates to create photonic hydrogels were reported.[199] DCMs' presented iridescence tunability from red to green upon drying, which shifts back to red rapidly after rehydration. The quick color change is attributed to the absence of the *N*-acetyl group after deacetylation, suggesting water interactions improvement in swelling and deswelling behaviors, implying that the membrane works as a responsive photonic polymer.

Chiral nitrogen-doped (N-doped) carbon porous materials can be produced from purified chitin membranes of crustacean exoskeletons for enantioselective adsorption.[196] The membranes were used to produce chiral hydrogels via calcium-mediated self-assembly, excusing chemical etching and templating before thermal treatment to afford the N-doped carbon structures. The carbonized material presented enantioselectivity over a racemic mixture by preferentially adsorbing D-lactic acid and producing 16.3% of enantiomeric excess of L-lactic acid, demonstrating the effectiveness in chiral separation. Lactic acid (LA) is a chiral natural compound existing in the L- and D-lactic acid enantiomeric forms and is also the monomeric

unit of polylactic acid (PLA). Industrial fermentation creates LA as a racemic mixture, whereas PLA is produced by employing only one enantiomer to enhance molecular packing or crystallinity. In other words, it is essential to resolve the LA racemate produced during the industrial process. Chitin-based materials may adsorb LA due to their alkaline nature, and their chiral geometries make them suitable for enantioselective adsorption.

Most of the research has focused on the photonic properties of cholesteric materials. However, their potential for manufacturing high-performance nanocomposites based on ChNCs has also been investigated. For instance, an electrically-assisted printing process was used to create a reinforced structure with anisotropic layers of aligned surface-modified multiwalled carbon nanotubes (MWCNT-S).[211] A rotating stage controls the alignment direction of MWCNTS, and the role of this stacking of layers to increase mechanical properties is investigated. A smaller rotation angle resulted in improved energy dissipation and impact resistance. Thin-ply *Carbon Fiber Reinforced Plastic* laminates were created, inspired by the helicoidal geometry of the dactyl club periodic area of the mantis shrimp.[212] However, an exception occurred and the non-lamellar nature of biological twisted plywood was not attained. Very small pitch angles are necessary to obtain the favorable damage mechanisms displayed by the twisted plywood construction.

Following the above sections, which were dedicated to the helicoidal cellulose and chitin molecular and nanostructures, in the next part of the work, helical cellulose systems at higher length scales are addressed.

8. Left-handed micro helices from vascular leaf petioles

Long helical cellulosic elements with several centimeters in length can be isolated from leaf petioles on a much higher length scale. Until now, only left-handed coils were isolated from the vascular conduits of several plant species petioles.[213] These coils can be collected by breaking the leaves and the cellulosic skeleton isolated by chemical treatment with alkali and acid chlorite.

The isolated helical thickenings were studied by polarized light microscopy, which allowed the determination of the dimensions and the handedness of the helices.[214] The helices were found to be birefringent, and after careful observation under an optical microscope between crossed polars with a 530 nm red retardation plate, cellulose was found to be oriented along the helices´main axis.[213,214] Vascular elements of celery isolated in water were found to be formed

by self-assembled filaments at the nanoscale. The surface morphologies of individual filaments were also observed by atomic force microscopy (AFM).[214] Fibrils inside the left-handed filaments seemed to form right-handed helices.[213,214] Moreover, AFM revealed the existence of randomly oriented nanorods with diameters of 3 nm, corresponding to the crystallite size of celery cellulose determined by X-ray diffraction.[214] Tracheary coils were isolated from different species of plants, and it was observed that they could be formed by single or multiple coils with two, three, or four individual filaments. Other studies indicate that the surface morphology of the filaments varies from plant to plant, which translates into different mechanical properties.[215] To analyze the surface of these filaments, atomic force microscopy and SEM remains the chosen techniques. However, more recently, nematic liquid crystal droplets suspended on the microfilaments, observed by polarizing optical microscopy (POM), were used to sense the surface morphology of helical microfilaments isolated from *A. africanus* and *O. thyrsoides* leaves species from the same *Asparagales* order. Nematic droplets pierced in *O. thyrsoides* showed a defect ring around the microfilament, contrasting with the ellipsoidal fringes observed for droplets suspended in filaments from *A. africanus*. The textures observed indicate a typical homeotropic anchoring for *A. africanus* tracheary microfilaments and a tangential anchoring, along the microfilament main axis, for filaments isolated from *O. thyrsoides*. AFM and stress/strain uniaxial tensile tests assessed the mechanical properties of the microfilaments. The elastic modulus and adhesion determined by AFM revealed the existence of different outer layers that granted more flexibility and less resistance to the microfilaments of *O. thyrsoides* compared with the rigidity and adhesion properties found for A. africanus microfilaments. Uniaxial mechanical tests revealed a higher value of Young´s modulus for *A. africanus* than *O. thyrsoides* filaments. This difference was mainly attributed to entanglements promoted by the smooth and rough surface morphologies of *O. thyrsoid* and *A. africanus* filaments, respectively.[215,216] It was shown that despite the helicity, shape, and common cellulose skeleton of microfilaments existing in the tracheary system of plant leaves, their interaction with the environment is crucial for their diverse mechanical behavior.[215,217]

Left-handed micro coils isolated from different vascular plant vessels were used as templates to prepare conducting[218] magnetic microswimmers.[7] Micro coils templates from the rhizome of *Nelumbo nucifera* (lotus) were used to fabricate silver-coated conducting springs.[218] Titanium/nickel helical microswimmers were also manufactured from coil vessels of *Rhaphiolepis indica*, *Agapanthus africanus*, *Cotoneaster lacteus*, *Passiflora edulis*, and *Musa acuminata*. These micro magnetic coils were found to move (250 μm/s) in organic fluids,

including human serum (**Figure 18**a and 18b).[7] Helical cellulose filaments from vascular plant vessels are soft, low-cost, biocompatible, and microswimmers[219] are great candidates for bio-applications.

9. Tendrils left and right-handed helices

On the length scale of millimeters, much larger than the helices from the vessels of plants, tendrils of climbing plants, such as in *Lathyrus spp.*, *Parthenocissus quinquefolia*, *Clematis vitalba*, *Vicia spp.*, and, *Bryonia alba* exhibit spirals, and helices (as shown in Figure 1 for *Passiflora edulis*). These long filaments possess a cellulose skeleton, and the helices and spirals develop from achiral millimetric straight filaments.[220] Despite the absence of chirality of the initial filament, the long tendrils curl into spirals if held by one end and into right and left-handed helices separated by a straight segment if held by both ends.[221]

Inspired by the shapes of tendrils, helical cellulose-based microfibers and jets were reported in the literature.[3,222] Liquid crystalline solutions were used as precursor solutions, and nuclear magnetic resonance imaging (MRI) and polarizing optical microscopy (POM) techniques were used to investigate the morphology and structure of fibers and jets.[3] It was found that the fibers and jets acquired intrinsic curvature during production due to the development of a core disclination running out of the main axis of the fibers and jets.[3] After these findings, inspired by asymmetric mechanisms, many studies were reported involving the production of curled fibers by different techniques and from other polymers. Among these systems, micro/nanofibers obtained by electrospinning have been reported.[223] Electrospinning allows the production of non-woven membranes built up from fibers with micro/nano diameters.[224–226] Briefly, electrospinning involves mainly applying an electric field to a polymer solution through a tip of a metallic needle.[227,228] The electric field causes the accumulation of electric charges at the tip of the needle, which originate in the formation of a cone at the end of the needle. When the value of the electric field overcomes the polymer solution's surface tension, a thin jet is produced from the cone shape. The jet travels toward a target promoting the solvent's evaporation and the filaments' stretching. The fibers are then collected on the target that can have different geometries and be made of diverse materials.[229–231] Several parameters can be optimized to obtain helices by electrospinning, including the percussor solutions' rheological behavior and the mechanical properties of the polymers involved. The intrinsic curvature of the microfibers can be achieved during the electrospinning process by coaxial and side-by-side electrospinning or after the preparation of the filaments. Coaxial electrospinning involves off-

centered core-shell spinnerets[232,233] and side-by-side using two polymers that contract differently after solvent removal.[234] To produce helices from straight electrospun filaments, these must-have chemical reactive sites. These sites can be selectively activated to form an asymmetry along the main axis of the filament.[235] The surface of these filaments can be smooth, as in young tendrils, or wrinkled, like the effect seen when the tendril ages and lignifies. Wrinkled asymmetric elastic filaments were prepared through two chemical paths. First, tri- and difunctional pre-polymers reacted to form elastic fibers, followed by UV irradiation of one-half of the filament to create a top layer more crosslinked than the bulk. Wrinkles develop in the top layer after extraction of the sol fraction in an appropriate solvent.[236]

Inspired by tendrils shapes and movements, Wei Wang et al.[237] created soft clamps from polymer-paper bilayer composite sheets with different patterns using 3D printing. These clamps were designed to imitate plant tendrils' bending, spiral, and helical movements, making them effective for lifting objects. The paper surface of the sheet provided excellent adhesion for the printed polymer, which was stretched during printing to store internal strain as memory. This memory strain was released upon heating, resulting in different shapes and movements depending on the printed geometry. By using these shapes and movements, the researchers were able to design clamps that could lift objects using movements similar to those of plant tendrils (Figure 18c).[237]

10. Movements at the macroscale from helicoidal plants' awns

Helicoidal cellulosic structures in plants were also reported to possess adaptive movements in response to environmental conditions, namely moisture. At the origin of these movements are stiff cellulose fibers immersed in soft matrices.[238] Noteworthy is reversible motions in plant dead tissues actuated by external stimulus. These movements indicate that programmed cellulosic structures remain active even after leaving the plant. Plants have been using, among other strategies, responsive dead tissues to disperse seeds. The mechanisms used to spread and self-drill seeds in the soil involve cellulose-based helicoidal structures, such as the awns of *Erodium* fruits. *Erodium* belongs to the *Geraniaceae* family, and each fruit is characterized by having five seeds attached to a long (compared with the length of the seed) hydrated cellulosic filament (awn) that is slightly twisted, as found by MRI, around a joint central dried cellulose-based stiff rod.[239] When the awn dries contracts, relative to the central cellulosic rod, and separates from the fruit transporting the seed in the air.[6,239–243] Once on the ground, the awn continues drying and forms a right-handed helix. When it is allowed to hydrate, the helix

unwinds, and the awn adopts the shape of a straight filament. These movements allow the self-burial of the *Erodium* seeds. The responsive helix, the active part, appears between the seed and the tail. The dimension of the cross-section of the awn narrows from the active part to the inactive tail. The helicoidal active part was studied by different techniques, which include LC-PolScope retardance imaging, Scanning electron microscopy (SEM), Small-angle X-ray scattering (SAXS), and POM. A tilted helix, with the axis at an angle to the long axis of the cells, was found responsible for the coiling of the awn.[6,240–243] Left-handed helices instead of straight hydrated awns were reported to appear when the awns were soaked in alkaline solutions.[239] Furthermore, gentle chemical treatments were used to isolate from the awns the helical left-handed wet ribbons, which switched to right-handed ribbons when dried.[239,240] The observed chirality inversion was explained by the chemical attack that did not destroy the imprinted helicoidal tilted structures at the nano/micro scale but made the cellulose network more accessible to water. At the macroscale, the treated ribbon contract and expand more than the cells of the pristine awns in the presence of water; as the tilted cellulosic helix is not destroyed, the reversal of the ribbon chirality occurs.[239]

It was proved that the isolated ribbons could be used as scaffolds to produce mesoporous silica solid helices.[239] Bioinspired self-drilling seed carriers were fabricated from thin wood sheets after chemical treatment and wet molding. Chemicals were first used to remove hemicellulose and lignin. The fabricated biocompatible, scalable, and low-cost awns were planned to work well on flat and rough soils and optimized to transport seeds from different plants (Figure 18d).[244]

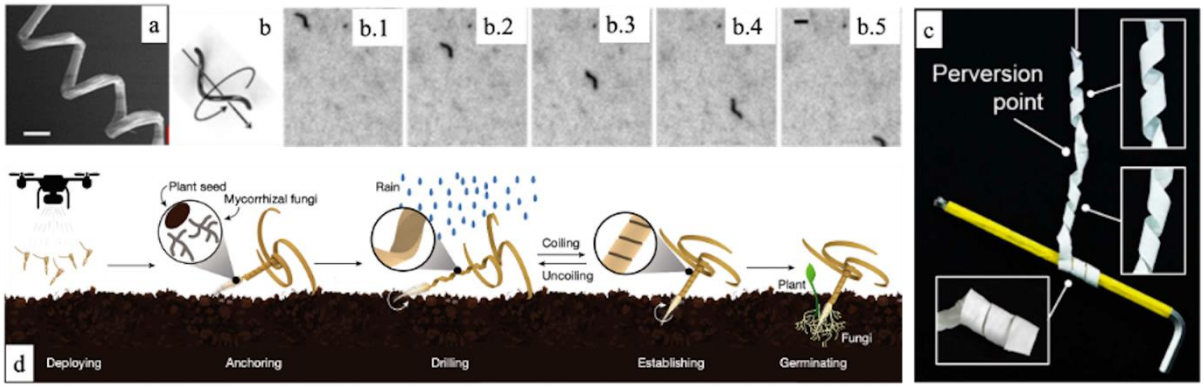

Figure 18. Bioinspired functional materials based on helicoidal plant structures. a) SEM image of a helical microswimmer from Rhaphiolepis indica leaves microfilaments after being coated with titanium and nickel nanolayers. Scale bar, 5 μm. b) Schematic of the corkscrew motion of the helical microswimmer, from b.1 to b.5 (600 ms intervals), in pure human serum by the action of a rotating magnetic field. Scale bar, 20 μm. a-b) Adapted with permission from [7]. Copyright © 2014, American Chemical Society. c) Synthetic helicoidal robot inspired by Cucumis tendril made from polyester and a sheet of paper lifting a rod (insets show the right

and left-handed helices of the stripe. Adapted with permission from [237]. Copyright © 2018, American Chemical Society. d) Steps from spreading to germination of three-tailed awns made from white oak lumbers, inspired in natural *Erodium guinum* movements. Reproduced with permission.[244] Copyright © 2023, The Author(s), under exclusive license to Springer Nature Limited..

11. Conclusion and a Twisted Future

Cellulose and chitin are renewable, non-toxic, and available, which makes them great candidates to replace oil-based polymers for many applications. We have shown that cellulose, its derivatives, and chitin can mimic some natural materials' helicoidal structures and functions. For instance, cellulose and chitin films produced from liquid crystalline solutions can self-assemble into colorful iridescent films with similar optical characteristics found in some plants and insects. Helical cellulose structures with selective circular polarized light reflection and transmission response were integrated into transistor devices, opening various applications, including optical fibers, communication, and imaging.

It was evidenced that reaction/diffusion mechanisms and the evaporation at boundaries could control the formation of the colorful patterns in quasi-2D liquid cellulose-based liquid crystalline samples. Cellulose/water interactions were found to determine the helicoidal handedness and pitch of the liquid crystalline phase. It was also evidenced that the liquid crystalline phase can be used to probe interactions between cellulose and water. Fundamental questions persist about better understanding the role of water in non-equilibrium systems and in the self-assembly process. All these systems inspire to the development of cellulose-based colorimetric timers, time-dependent dynamical coloration, and their use for camouflage.

Contrary to chitin derivatives, such as chitosan, which has been widely explored, chitin helicoidal self-assembled structures are expected to give rise to new functional materials in the near future, in this sense, chitin extraction procedures must be improved.

Another interesting field of research with technological applications concerns the response of helical cellulose-based structures to external stimuli, for example, moisture. In fact, the interplay between cellulose and water greatly influences the helical structures at the micro and millimeter length scales. Responsive cellulosic helical structures to humidity are at the genesis of the production of self-burial systems that are suggested to be used for the reforestation of lands after, for example, a fire. Furthermore, among the technological applications of these responsive anisotropic structures are the development of autonomous micro and nanomachines and systems for energy harvesting. In addition, nonwoven membranes with shape-responsive nano and micro helical fibers are ideal for capturing water from the atmosphere, which is crucial

for populations living in arid regions or countries subject to periods of drought. Self-cleaning membranes can be idealized for water purification. Helical shapes are also a source of templates for conducting wires for electronic devices.

Mimicking the twisted designs of cellulosic structures and using cellulose-based materials to obtain objects used in everyday life are challenging fields of research and technology. For example, cups, bottles, and other recipients with helical shapes that are easier to ply and recycle from less material are target objects to replace oil-based materials such as water bottles with twisted designs existing in the market.

Overall, the potential of helical structures made from cellulose and chitin is vast and promising, with applications ranging from material science to biotechnology. More exciting and innovative applications for these unique structures will likely emerge as research in this area progresses.

Acknowledgements

This work was financed by national funds from FCT—Fundação para a Ciência e a Tecnologia, I.P., in the scope of the projects LA/P/0037/2020, UIDP/50025/2020 and UIDB/50025/2020 of the Associate Laboratory Institute of Nanostructures, Nanomodelling and Nanofabrication—i3N. European Cooperation in Science & Technology (COST) Action: CA21159 - Understanding interaction light - biological surfaces: possibility for new electronic materials and devices (PhoBioS). All the authors contributed to the manuscript's writing, improvement, and editing.

References

[1] T. A. Gorshkova, P. V. Mikshina, O. P. Gurjanov, S. B. Chemikosova, *Biochem.* **2010**, *75*, 159.

[2] P. Purushotham, R. Ho, J. Zimmer, *Science* **2020**, *369*, 1089.

[3] M. H. Godinho, J. P. Canejo, G. Feio, E. M. Terentjev, *Soft Matter* **2010**, *6*, 5965.

[4] S. Vignolini, P. J. Rudall, A. V. Rowland, A. Reed, E. Moyroud, R. B. Faden, J. J. Baumberg, B. J. Glover, U. Steiner, *Proc. Natl. Acad. Sci.* **2012**, *109*, 15712.

[5] A. G. Dumanli, G. Kamita, J. Landman, H. van der Kooij, B. J. Glover, J. J. Baumberg, U. Steiner, S. Vignolini, *Adv. Opt. Mater.* **2014**, *2*, 646.

[6] H. Aharoni, Y. Abraham, R. Elbaum, E. Sharon, R. Kupferman, *Phys. Rev. Lett.* **2012**, *108*, 238106.

[7] W. Gao, X. Feng, A. Pei, C. R. Kane, R. Tam, C. Hennessy, J. Wang, *Nano Lett.* **2014**,

14, 305.

[8] B. Cho, D. Kim, T. Kim, *Sci. Rep.* **2022**, *12*, 11816.

[9] S. N. Fernandes, L. F. Lopes, M. H. Godinho, *Curr. Opin. Solid State Mater. Sci.* **2019**, *23*, 63.

[10] J. Lv, X. Lv, M. Ma, D.-H. Oh, Z. Jiang, X. Fu, *Carbohydr. Polym.* **2023**, *299*, 120142.

[11] G. Crini, *Environ. Chem. Lett.* **2019**, *17*, 1623.

[12] M. N. V. R. Kumar, *React. Funct. Polym.* **2000**, *46*, 1.

[13] D. H. Bartlett, F. Azam, *Science* **2005**, *310*, 1775.

[14] Y. Bouligand, M. O. Soyer, S. Puiseux-Dao, *Chromosoma* **1968**, *24*, 251.

[15] A. C. Neville, D. C. Gubb, R. M. Crawford, *Protoplasma* **1976**, *90*, 307.

[16] Y. Bouligand, *Le J. Phys. Colloq.* **1975**, *36*, C1.

[17] H. Fabritius, C. Sachs, D. Raabe, S. Nikolov, M. Friák, J. Neugebauer, In *Chitin: Formation and Diagenesis* (Ed.: Gupta, N. S.), Springer Netherlands, Dordrecht, **2011**, pp. 35–60.

[18] P. Drach, *C.R. Acad. Sci. Paris* **1953**, *237*, 1772.

[19] Y. Bouligand, *C.R. Acad. Sci. Paris* **1965**, *261*, 3665.

[20] Y. Bouligand, *Tissue Cell* **1972**, *4*, 189.

[21] Y. Bouligand, *Le J. Phys. Colloq.* **1969**, *30*, C4.

[22] M. M. Giraud-Guille, *Int. Rev. Cytol.* **1996**, *166*, 59.

[23] A. C. Neville, *Biology of the Arthropod Cuticle*, Springer Berlin Heidelberg, Berlin, Heidelberg, **1975**.

[24] E. Belamie, G. Mosser, F. Gobeaux, M. M. Giraud-Guille, *J. Phys. Condens. Matter* **2006**, *18*, S115.

[25] M.-M. Giraud-Guille, *Tissue Cell* **1986**, *18*, 603.

[26] J. de Gennes, P.-G.; Prost, *The Physics of Liquid Crystals*, Claredon Press Oxford, **1993**.

[27] P. Oswald, P. Pieranski, *Nematic and Cholesteric Liquid Crystals*, 1st ed., CRC Press, Taylor and Francis, London, **2005**.

[28] M. H. Godinho, *Science* **2020**, *369*, 918.

[29] H. de Vries, *Acta Crystallogr.* **1951**, *4*, 219.

[30] Y. Bouligand, F. Livolant, *J. Phys.* **1984**, *45*, 1899.

[31] F. Livolant, *Phys. A Stat. Mech. its Appl.* **1991**, *176*, 117.

[32] J. P. Canejo, N. Monge, C. Echeverria, S. N. Fernandes, M. H. Godinho, *Liq. Cryst. Rev.* **2017**, *5*, 86.

[33] O. D. Lavrentovich, M. Kleman, In *Chirality in Liquid Crystals* (Eds.: Kitzerow, H.-S.; Bahr, C.), Springer-Verlag, New York, **2001**, pp. 115–158.

[34] G. Strout, S. D. Russell, D. P. Pulsifer, S. Erten, A. Lakhtakia, D. W. Lee, *Ann. Bot.* **2013**, *112*, 1141.

[35] R. M. Graham, D. W. Lee, K. Norstog, *Am. J. Bot.* **1993**, *80*, 198.

[36] L. M. Steiner, Y. Ogawa, V. E. Johansen, C. R. Lundquist, H. Whitney, S. Vignolini, *Interface Focus* **2018**, *9*, 20180055.

[37] T. Boonkerd, *Blumea J. Plant Taxon. Plant Geogr.* **2006**, *51*, 143.

[38] S. Vignolini, T. Gregory, M. Kolle, A. Lethbridge, E. Moyroud, U. Steiner, B. J. Glover, P. Vukusic, P. J. Rudall, *J. R. Soc. Interface* **2016**, *13*, 20160645.

[39] D. W. Lee, *Nature* **1991**, *349*, 260.

[40] E. Cazetta, L. S. Zumstein, T. A. Melo-Júnior, M. Galetti, *Rev. Bras. Botânica* **2008**, *31*, 303.

[41] R. B. Foster, Field Museum, *Margaritaria nobilis L.f.*, https://plantidtools.fieldmuseum.org/en/nlp/catalogue/3669879, accessed: March, **2023**.

[42] M. Kolle, A. Lethbridge, M. Kreysing, J. J. Baumberg, J. Aizenberg, P. Vukusic, *Adv. Mater.* **2013**, *25*, 2239.

[43] R. Middleton, E. Moyroud, P. J. Rudall, C. J. Prychid, M. Conejero, B. J. Glover, S. Vignolini, *New Phytol.* **2021**, *230*, 2327.

[44] L. Solhi, V. Guccini, K. Heise, I. Solala, E. Niinivaara, W. Xu, K. Mihhels, M. Kröger, Z. Meng, J. Wohlert, H. Tao, E. D. Cranston, E. Kontturi, *Chem. Rev.* **2023**, *123*, 1925.

[45] A. Etale, A. J. Onyianta, S. R. Turner, S. J. Eichhorn, *Chem. Rev.* **2023**, *123*, 2016.

[46] Z. A. Popper, G. Michel, C. Hervé, D. S. Domozych, W. G. T. Willats, M. G. Tuohy, B. Kloareg, D. B. Stengel, *Annu. Rev. Plant Biol.* **2011**, *62*, 567.

[47] P. Sarkar, E. Bosneaga, M. Auer, *J. Exp. Bot.* **2009**, *60*, 3615.

[48] S. Li, L. Bashline, L. Lei, Y. Gu, *Arab. B.* **2014**, *12*, e0169.

[49] G. Guerriero, J. Fugelstad, V. Bulone, *J. Integr. Plant Biol.* **2010**, *52*, 161.

[50] D. J. Cosgrove, *Plant Physiol.* **2022**, *189*, 1246.

[51] Z. Qiao, E. R. Lampugnani, X.-F. Yan, G. A. Khan, W. G. Saw, P. Hannah, F. Qian, J. Calabria, Y. Miao, G. Grüber, S. Persson, Y.-G. Gao, *Proc. Natl. Acad. Sci.* **2021**, *118*, e2024015118.

[52] Y. Li, M. Lin, J. W. Davenport, *J. Phys. Chem. C* **2011**, *115*, 11533.

[53] A. Paajanen, S. Ceccherini, T. Maloney, J. A. Ketoja, *Cellulose* **2019**, *26*, 5877.

[54] L. Bu, M. E. Himmel, M. F. Crowley, *Carbohydr. Polym.* **2015**, *125*, 146.

[55] K. Conley, L. Godbout, M. A. Whitehead, T. G. M. van de Ven, *Carbohydr. Polym.* **2016**, *135*, 285.

[56] H. O'Neill, S. V. Pingali, L. Petridis, J. He, E. Mamontov, L. Hong, V. Urban, B. Evans, P. Langan, J. C. Smith, B. H. Davison, *Sci. Rep.* **2017**, *7*, 11840.

[57] J. A. Hadden, A. D. French, R. J. Woods, *Biopolymers* **2013**, *99*, 746.

[58] P. A. Penttilä, A. Paajanen, J. A. Ketoja, *Carbohydr. Polym.* **2021**, *251*, 117064.

[59] A. Chami Khazraji, S. Robert, *J. Nanomater.* **2013**, *2013*, 1.

[60] T. Zimmermann, E. Pöhler, T. Geiger, *Adv. Eng. Mater.* **2004**, *6*, 754.

[61] P. Chen, J. Wohlert, L. Berglund, I. Furó, *J. Phys. Chem. Lett.* **2022**, *13*, 5424.

[62] E. L. Lindh, C. Terenzi, L. Salmén, I. Furó, *Phys. Chem. Chem. Phys.* **2017**, *19*, 4360.

[63] S. P. Rowland, E. J. Roberts, *J Polym Sci Part A-1 Polym Chem* **1972**, *10*, 2447.

[64] J. F. Revol, H. Bradford, J. Giasson, R. H. Marchessault, D. G. Gray, *Int. J. Biol. Macromol.* **1992**, *14*, 170.

[65] S. J. Eichhorn, *Soft Matter* **2011**, *7*, 303.

[66] S. Beck-Candanedo, M. Roman, D. G. Gray, *Biomacromolecules* **2005**, *6*, 1048.

[67] D. Klemm, F. Kramer, S. Moritz, T. Lindström, M. Ankerfors, D. Gray, A. Dorris, *Angew. Chemie Int. Ed.* **2011**, *50*, 5438.

[68] W. Y. Hamad, *Cellulose nanocrystals: Properties, production and applications*, John Wiley & Sons Ltd, West Sussex, United Kingdom **2017**.

[69] A. Yurtsever, P.-X. Wang, F. Priante, Y. Morais Jaques, K. Miyazawa, M. J. MacLachlan, A. S. Foster, T. Fukuma, *Sci. Adv.* **2022**, *8*, 160.

[70] L. Onsager, *Ann. N. Y. Acad. Sci.* **1949**, *51*, 627.

[71] J. Revol, R. H. Marchessaultf, *Int. J. Biol. Macromol.* **1993**, *15*, 329.

[72] J. P. F. Lagerwall, C. Schütz, M. Salajkova, J. Noh, J. H. Park, G. Scalia, L. Bergström, *NPG Asia Mater.* **2014**, *6*, 1.

[73] P.-X. Wang, M. J. MacLachlan, *Philos. Trans. R. Soc. A Math. Phys. Eng. Sci.* **2018**, *376*, 20170042.

[74] C. Schütz, J. R. Bruckner, C. Honorato-Rios, Z. Tosheva, M. Anyfantakis, J. P. F. Lagerwall, *Crystals* **2020**, *10*, 199.

[75] Y.-K. Kim, S. V. Shiyanovskii, O. D. Lavrentovich, *J. Phys. Condens. Matter* **2013**, *25*, 404202.

[76] H. Zocher, *Zeitschrift für Anorg. und Allg. Chemie* **1925**, *147*, 91.

[77] K. Coper, H. Freundlich, *Trans. Faraday Soc.* **1937**, *33*, 348.

[78] P. W. Oakes, J. Viamontes, J. X. Tang, *Phys. Rev. E - Stat. Nonlinear, Soft Matter Phys.* **2007**, *75*, 1.

[79] I. Langmuir, *J. Chem. Phys.* **1938**, *6*, 873.

[80] H. Zocher, K. Jacobsohn, *Kolloidchem. Beihefte* **1929**, *28*, 167.

[81] H. Zocher, C. Török, *Kolloid-Zeitschrift* **1960**, *170*, 140.

[82] D. Gray, *Nanomaterials* **2016**, *6*, 213.

[83] I. Usov, G. Nyström, J. Adamcik, S. Handschin, C. Schütz, A. Fall, L. Bergström, R. Mezzenga, *Nat. Commun.* **2015**, *6*, 7564.

[84] X. Qin, B. C. Marchi, Z. Meng, S. Keten, *Nanoscale Adv.* **2019**, *1*, 1351.

[85] B. Natarajan, J. W. Gilman, *Philos. Trans. R. Soc. A Math. Phys. Eng. Sci.* **2018**, *376*, 20170050.

[86] P.-X. Wang, W. Y. Hamad, M. J. MacLachlan, *Nat. Commun.* **2016**, *7*, 11515.

[87] O. O'Keeffe, P. X. Wang, W. Y. Hamad, M. J. Maclachlan, *J. Phys. Chem. Lett.* **2019**, *10*, 278.

[88] A. Abbasi Moud, *ACS Omega* **2022**, *7*, 30673.

[89] G. Nyström, M. Arcari, J. Adamcik, I. Usov, R. Mezzenga, *ACS Nano* **2018**, *12*, 5141.

[90] T. G. Parton, R. M. Parker, G. T. van de Kerkhof, A. Narkevicius, J. S. Haataja, B. Frka-Petesic, S. Vignolini, *Nat. Commun.* **2022**, *13*, 2657.

[91] R. R. da Rosa, P. E. S. Silva, D. V. Saraiva, A. Kumar, A. P. M. de Sousa, P. Sebastião, S. N. Fernandes, M. H. Godinho, *Adv. Mater.* **2022**, *34*, 2108227.

[92] A. P. C. Almeida, J. P. Canejo, S. N. Fernandes, C. Echeverria, P. L. Almeida, M. H. Godinho, *Adv. Mater.* **2018**, *30*, 1703655.

[93] A. Tran, W. Y. Hamad, M. J. MacLachlan, *Langmuir* **2018**, *34*, 646.

[94] A. Tran, W. Y. Hamad, M. J. MacLachlan, *ACS Appl. Nano Mater.* **2018**, *1*, 3098.

[95] C. Honorato-Rios, C. Lehr, C. Schütz, R. Sanctuary, M. A. Osipov, J. Baller, J. P. F. Lagerwall, *NPG Asia Mater.* **2018**, *10*, 455.

[96] B. E. Droguet, H. L. Liang, B. Frka-Petesic, R. M. Parker, M. F. L. De Volder, J. J. Baumberg, S. Vignolini, *Nat. Mater.* **2022**, *21*, 352.

[97] M. Giese, L. K. Blusch, M. K. Khan, M. J. MacLachlan, *Angew. Chemie - Int. Ed.* **2015**, *54*, 2888.

[98] D. V. Saraiva, R. Chagas, B. M. de Abreu, C. N. Gouveia, P. E. S. Silva, M. H. Godinho, S. N. Fernandes, *Crystals* **2020**, *10*, 122.

[99] K. Yao, Q. Meng, V. Bulone, Q. Zhou, *Adv. Mater.* **2017**, *29*, 1701323.

[100] A. Tran, C. E. Boott, M. J. MacLachlan, *Adv. Mater.* **2020**, *32*, 1905876.

[101] R. M. Parker, G. Guidetti, C. A. Williams, T. Zhao, A. Narkevicius, S. Vignolini, B. Frka-Petesic, *Adv. Mater.* **2018**, *30*, 1704477.

[102] D. Qu, O. J. Rojas, B. Wei, E. Zussman, *Adv. Opt. Mater.* **2022**, *10*, 2201201.

[103] S. N. Fernandes, J. P. Canejo, C. Echeverria, M. H. Godinho, In *Liquid Crystalline Polymers*, Springer International Publishing, Cham, **2015**, pp. 339–368.

[104] R. S. Werbowyj, D. G. Gray, *Mol Cryst Liq Cryst* **1976**, *34*, 97.

[105] R. S. Werbowyj, D. G. Gray, *Macromolecules* **1984**, *17*, 1512.

[106] M. H. Godinho, D. G. Gray, P. Pieranski, *Liq. Cryst.* **2017**, *44*, 2108.

[107] K. Shimamura, J. L. White, J. F. Fellers, *J. Appl. Polym. Sci.* **1981**, *26*, 2165.

[108] G. Charlet, D. G. Gray, *Macromolecules* **1987**, *20*, 33.

[109] P. Zugenmaier, In *Handbook of Liquid Crystals*, Wiley-VCH Verlag GmbH & Co. KGaA, Weinheim, Germany, **2014**, pp. 1–39.

[110] P. Zugenmaier, P. Haurand, *Carbohydr. Res.* **1987**, *160*, 369.

[111] U. Vogt, P. Zugenmaier, *Berichte der Bunsengesellschaft für Phys. Chemie* **1985**, *89*, 1217.

[112] J. X. Guo, D. G. Gray, *Macromolecules* **1989**, *22*, 2082.

[113] J. X. Guo, D. G. Gray, *Macromolecules* **1989**, *22*, 2086.

[114] P. Ohlendorf, A. Greiner, *Polym. Chem.* **2015**, *6*, 2734.

[115] H. Ishii, K. Sugimura, Y. Nishio, *Cellulose* **2019**, *26*, 399.

[116] H.-L. Liang, M. M. Bay, R. Vadrucci, C. H. Barty-King, J. Peng, J. J. Baumberg, M. F. L. De Volder, S. Vignolini, *Nat. Commun.* **2018**, *9*, 4632.

[117] J. Wei, X. Aeby, G. Nyström, *Adv. Mater. Technol.* **2023**, *8*, 2200897.

[118] T. Balcerowski, B. Ozbek, O. Akbulut, A. G. Dumanli, *Small* **2023**, *19*, 2205506.

[119] S. Suto, K. Suzuki, *Polymer* **1997**, *38*, 391.

[120] S. Ming, X. Zhang, C. L. C. Chan, Z. Wang, M. M. Bay, R. M. Parker, S. Vignolini, *Adv. Sustain. Syst.* **2023**, *2200469*, 1.

[121] C. L. C. Chan, I. M. Lei, G. T. van de Kerkhof, R. M. Parker, K. D. Richards, R. C. Evans, Y. Y. S. Huang, S. Vignolini, *Adv. Funct. Mater.* **2022**, *32*.

[122] Z. Zhang, C. Wang, Q. Wang, Y. Zhao, L. Shang, *Proc. Natl. Acad. Sci. U. S. A.* **2022**, *119*, 1.

[123] K. George, M. Esmaeili, J. Wang, N. Taheri-Qazvini, A. Abbaspourrad, M. Sadati, *Proc.*

Natl. Acad. Sci. **2023**, *120*, 1.

[124] A. M. Ritcey, D. G. Gray, *Biopolymers* **1988**, *27*, 1363.

[125] R. Chagas, P. E. S. Silva, S. N. Fernandes, S. Žumer, M. H. Godinho, *Faraday Discuss.* **2020**, *223*, 247.

[126] X. Mu, D. G. Gray, *Cellulose* **2015**, *22*, 1103.

[127] B. D. Wilts, V. Saranathan, *Small* **2018**, *14*, 1802328.

[128] R. O. Prum, S. Williamson, *Proc. R. Soc. B Biol. Sci.* **2002**, *269*, 781.

[129] P. E. S. Silva, R. Chagas, S. N. Fernandes, P. Pieranski, R. L. B. Selinger, M. H. Godinho, *Commun. Mater.* **2021**, *2*, 79.

[130] A. J. Ackroyd, G. Holló, H. Mundoor, H. Zhang, O. Gang, I. I. Smalyukh, I. Lagzi, E. Kumacheva, *Sci. Adv.* **2021**, *7*, 1.

[131] G. Kamita, S. Vignolini, A. G. Dumanli, *Nanoscale Horizons* **2023**, *8*, 887.

[132] A. R. Parker, *Proc. R. Soc. B Biol. Sci.* **1998**, *265*, 967.

[133] A. Parker, *In The Blink Of An Eye: How Vision Sparked The Big Bang Of Evolution*, Basic Books, New York, **2004**.

[134] A. R. Parker, *Opt. Laser Technol.* **2011**, *43*, 323.

[135] F. Zhao, D. J. Bottjer, S. Hu, Z. Yin, M. Zhu, *Sci. Rep.* **2013**, *3*, 2751.

[136] M. E. McNamara, D. E. G. Briggs, P. J. Orr, H. Noh, H. Cao, *Proc. R. Soc. B Biol. Sci.* **2012**, *279*, 1114.

[137] Y. Ma, C. Guo, N. Dai, J. Shen, J. Guan, *J. Mech. Behav. Biomed. Mater.* **2022**, *125*, 104954.

[138] https://www.hlmd.de/museum/forschung/naturgeschichte/dr-torsten-wappler.html.

[139] http://www.living-jewels.com/chrysina_gloriosa.htm. © Poul Beckmann. — *The copyright holder of this work allows anyone to use it for any purpose including unrestricted redistribution, commercial use, and modification.*

[140] P. Vukusic, J. R. Sambles, *Nature* **2003**, *424*, 852.

[141] L. P. Biró, J. P. Vigneron, *Laser Photonics Rev.* **2011**, *5*, 27.

[142] G. Horváth, D. Varjú, *Polarized Light in Animal Vision*, Springer Berlin Heidelberg, Berlin, Heidelberg, **2004**.

[143] D. J. Kemp, *Proc. R. Soc. B Biol. Sci.* **2007**, *274*, 1043.

[144] A. Loyau, D. Gomez, B. Moureau, M. Théry, N. S. Hart, M. Saint Jalme, A. T. D. Bennett, G. Sorci, *Behav. Ecol.* **2007**, *18*, 1123.

[145] A. B. Bond, A. C. Kamil, *Nature* **2002**, *415*, 609.

[146] W. H. Wente, J. B. Phillips, *Am. Nat.* **2003**, *162*, 461.

[147] K. Kertész, Z. Bálint, Z. Vértesy, G. I. Márk, V. Lousse, J. P. Vigneron, M. Rassart, L. P. Biró, *Phys. Rev. E - Stat. Nonlinear, Soft Matter Phys.* **2006**, *74*, 021922.

[148] G. D. Ruxton, T. N. Sherratt, M. P. Speed, *Avoiding Attack: The Evolutionary Ecology of Crypsis, Warning Signals and Mimicry*, Oxford University PressOxford, Oxford, **2004**.

[149] S. Kinoshita, S. Yoshioka, *ChemPhysChem* **2005**, *6*, 1442.

[150] S. Molesky, Z. Lin, A. Y. Piggott, W. Jin, J. Vucković, A. W. Rodriguez, *Nat. Photonics* **2018**, *12*, 659.

[151] M. Eder, S. Amini, P. Fratzl, *Science* **2018**, *362*, 543.

[152] M. A. Barry, V. Berthier, B. D. Wilts, M.-C. Cambourieux, P. Bennet, R. Pollès, O. Teytaud, E. Centeno, N. Biais, A. Moreau, *Sci. Rep.* **2020**, *10*, 12024.

[153] A. E. Seago, P. Brady, J.-P. Vigneron, T. D. Schultz, *J. R. Soc. Interface* **2009**, *6*, S165.

[154] J. Sun, B. Bhushan, *RSC Adv.* **2012**, *2*, 12606.

[155] S. Tadepalli, J. M. Slocik, M. K. Gupta, R. R. Naik, S. Singamaneni, *Chem. Rev.* **2017**, *117*, 12705.

[156] S. Caveney, *Proc. R. Soc. London. Ser. B. Biol. Sci.* **1971**, *178*, 205.

[157] S. Kinoshita, S. Yoshioka, J. Miyazaki, *Reports Prog. Phys.* **2008**, *71*, 076401.

[158] A. Matranga, S. Baig, J. Boland, C. Newton, T. Taphouse, G. Wells, S. Kitson, *Adv. Mater.* **2013**, *25*, 520.

[159] S. N. Fernandes, P. L. Almeida, N. Monge, L. E. Aguirre, D. Reis, C. L. P. de Oliveira, A. M. F. Neto, P. Pieranski, M. H. Godinho, *Adv. Mater.* **2017**, *29*, 1603560.

[160] L. Wang, A. M. Urbas, Q. Li, *Adv. Mater.* **2020**, *32*, 1801335.

[161] M. Mitov, *Adv. Mater.* **2012**, *24*, 6260.

[162] D. H. Goldstein, *Appl. Opt.* **2006**, *45*, 7944.

[163] R. Hegedüs, G. Szél, G. Horváth, *Vision Res.* **2006**, *46*, 2786.

[164] D. E. Azofeifa, M. Hernández-Jiménez, E. Libby, A. Solís, C. Barboza-Aguilar, W. E. Vargas, *J. Quant. Spectrosc. Radiat. Transf.* **2015**, *160*, 63.

[165] W. E. Vargas, M. Hernández-Jiménez, E. Libby, D. E. Azofeifa, Á. Solis, C. Barboza-Aguilar, *EPL* **2015**, *111*, 64001.

[166] A. Jullien, M. Neradovskiy, M. Mitov, *APL Photonics* **2020**, *5*, 096102.

[167] G. Agez, C. Bayon, M. Mitov, *Acta Biomater.* **2017**, *48*, 357.

[168] D. Raabe, C. Sachs, P. Romano, *Acta Mater.* **2005**, *53*, 4281.

[169] A. Jullien, M. Neradovskiy, A. Scarangella, M. Mitov, *J. R. Soc. Interface* **2020**, *17*, 20200239.

[170] P. Bouchal, J. Kapitán, M. Konečný, M. Zbončák, Z. Bouchal, *APL Photonics* **2019**, *4*, 126102.

[171] S. N. Khonina, N. L. Kazanskiy, S. V. Karpeev, M. A. Butt, *Micromachines* **2020**, *11*, 997.

[172] S. Lee, H. Kim, Y. Jeong, *Opt. Express* **2021**, *29*, 37712.

[173] J. Kobashi, H. Yoshida, M. Ozaki, *Sci. Rep.* **2017**, *7*, 16470.

[174] A. Scarangella, V. Soldan, M. Mitov, *Nat. Commun.* **2020**, *11*, 4108.

[175] L. T. McDonald, E. D. Finlayson, B. D. Wilts, P. Vukusic, *Interface Focus* **2017**, *7*, 20160129.

[176] G. Jacucci, O. D. Onelli, A. De Luca, J. Bertolotti, R. Sapienza, S. Vignolini, *Interface Focus* **2019**, *9*, 20180050.

[177] W. Suginta, P. Khunkaewla, A. Schulte, *Chem. Rev.* **2013**, *113*, 5458.

[178] J. Kadokawa, *RSC Adv.* **2015**, *5*, 12736.

[179] T.-D. Nguyen, M. J. MacLachlan, *Adv. Opt. Mater.* **2014**, *2*, 1031.

[180] S. Sviben, O. Spaeker, M. Bennet, M. Albéric, M. Albéric, J. H. Dirks, J. H. Dirks, B. Moussian, P. Fratzl, L. Bertinetti, Y. Politi, *ACS Appl. Mater. Interfaces* **2020**, *12*, 25581.

[181] http://www.tiermotive.de/%20Lizenz. © Jonathan Hornung (CC BY-SA 2.0 DE).

[182] H. Merzendorfer, L. Zimoch, *J. Exp. Biol.* **2003**, *206*, 4393.

[183] J. C. Weaver, G. W. Milliron, A. Miserez, K. Evans-Lutterodt, S. Herrera, I. Gallana, W. J. Mershon, B. Swanson, P. Zavattieri, E. DiMasi, D. Kisailus, *Science* **2012**, *336*, 1275.

[184] A. Al-Sawalmih, C. Li, S. Siegel, H. Fabritius, S. Yi, D. Raabe, P. Fratzl, O. Paris, *Adv. Funct. Mater.* **2008**, *18*, 3307.

[185] H. O. Fabritius, C. Sachs, P. R. Triguero, D. Raabe, *Adv. Mater.* **2009**, *21*, 391.

[186] I. M. Daly, M. J. How, J. C. Partridge, S. E. Temple, N. J. Marshall, T. W. Cronin, N. W. Roberts, *Nat. Commun.* **2016**, *7*, 12140.

[187] K. J. Kramer, T. L. Hopkins, J. Schaefer, *Insect Biochem. Mol. Biol.* **1995**, *25*, 1067.

[188] Y. N. Tan, P. P. Lee, W. N. Chen, *Fermentation* **2020**, *6*, 40.

[189] A. Domard, *Carbohydr. Polym.* **2011**, *84*, 696.

[190] X. Zhang, M. Rolandi, *J. Mater. Chem. B* **2017**, *5*, 2547.

[191] C. K. S. Pillai, W. Paul, C. P. Sharma, *Prog. Polym. Sci.* **2009**, *34*, 641.

[192] L. Bai, L. Liu, M. Esquivel, B. L. Tardy, S. Huan, X. Niu, S. Liu, G. Yang, Y. Fan, O. J.

Rojas, *Chem. Rev.* **2022**, *122*, 11604.

[193] E. Lizundia, T. D. Nguyen, R. J. Winnick, M. J. MacLachlan, *J. Mater. Chem. C* **2021**, *9*, 796.

[194] O. Kose, A. Tran, L. Lewis, W. Y. Hamad, M. J. MacLachlan, *Nat. Commun.* **2019**, *10*, 510.

[195] Y. Zhang, G. Liu, X. Yao, S. Gao, J. Xie, H. Xu, N. Lin, *Cellulose* **2018**, *25*, 3861.

[196] H. L. Nguyen, S. Ju, L. T. Hao, T. H. Tran, H. G. Cha, Y. J. Cha, J. Park, S. Y. Hwang, D. K. Yoon, D. S. Hwang, D. X. Oh, *ChemSusChem* **2019**, *12*, 3236.

[197] Y. Wu, K. Ye, Z. Liu, B. Wang, C. Yan, Z. Wang, C. Te Lin, N. Jiang, J. Yu, *ACS Appl. Mater. Interfaces* **2019**, *11*, 44700.

[198] I. Capasso, B. Liguori, L. Verdolotti, D. Caputo, M. Lavorgna, E. Tervoort, *Sci. Rep.* **2020**, *10*, 612.

[199] T. D. Nguyen, B. U. Peres, R. M. Carvalho, M. J. MacLachlan, *Adv. Funct. Mater.* **2016**, *26*, 2875.

[200] H. Sashiwa, S. I. Aiba, *Prog. Polym. Sci.* **2004**, *29*, 887.

[201] H. El Knidri, R. Belaabed, A. Addaou, A. Laajeb, A. Lahsini, *Int. J. Biol. Macromol.* **2018**, *120*, 1181.

[202] H. Van Duong, T. T. L. Chau, N. T. T. Dang, F. Vanterpool, M. Salmerón-Sánchez, E. Lizundia, H. T. Tran, L. V. Nguyen, T. D. Nguyen, *ACS Omega* **2018**, *3*, 86.

[203] N. Jana, D. Parbat, B. Mondal, S. Das, U. Manna, *J. Mater. Chem. A* **2019**, *7*, 9120.

[204] T. D. Nguyen, K. E. Shopsowitz, M. J. MacLachlan, *J. Mater. Chem. A* **2014**, *2*, 5915.

[205] D. X. Oh, Y. J. Cha, H.-L. Nguyen, H. H. Je, Y. S. Jho, D. S. Hwang, D. K. Yoon, *Sci. Rep.* **2016**, *6*, 23245.

[206] T. Philibert, B. H. Lee, N. Fabien, *Appl. Biochem. Biotechnol.* **2017**, *181*, 1314.

[207] A. G. Dumanli, T. Savin, *Chem. Soc. Rev.* **2016**, *45*, 6698.

[208] E. Belamie, P. Davidson, M. M. Giraud-Guille, *J. Phys. Chem. B* **2004**, *108*, 14991.

[209] A. Narkevicius, L. M. Steiner, R. M. Parker, Y. Ogawa, B. Frka-Petesic, S. Vignolini, *Biomacromolecules* **2019**, *20*, 2830.

[210] A. Narkevicius, R. M. Parker, J. Ferrer-Orri, T. G. Parton, Z. Lu, G. T. van de Kerkhof, B. Frka-Petesic, S. Vignolini, *Adv. Mater.* **2022**, *34*, 2203300.

[211] Y. Yang, Z. Chen, X. Song, Z. Zhang, J. Zhang, K. K. Shung, Q. Zhou, Y. Chen, *Adv. Mater.* **2017**, *29*, 1605750.

[212] L. Mencattelli, S. T. Pinho, *Compos. Sci. Technol.* **2019**, *182*, 107684.

[213] D. G. Gray, *Botany* **2020**, *98*, 77.

[214] D. G. Gray, *Cellulose* **2014**, *21*, 3181.

[215] A. P. Almeida, J. Canejo, U. Mur, S. Copar, P. L. Almeida, S. Žumer, M. H. Godinho, *Proc. Natl. Acad. Sci. U. S. A.* **2019**, *116*, 13188.

[216] J. Read, G. D. Sanson, *New Phytol.* **2003**, *160*, 81.

[217] C. T. McKee, J. A. Last, P. Russell, C. J. Murphy, *Tissue Eng. - Part B Rev.* **2011**, *17*, 155.

[218] K. Kamata, S. Suzuki, M. Ohtsuka, M. Nakagawa, T. Iyoda, A. Yamada, *Adv. Mater.* **2011**, *23*, 5509.

[219] G. Yan, A. A. Solovev, G. Huang, J. Cui, Y. Mei, *Curr. Opin. Colloid Interface Sci.* **2022**, *61*, 101609.

[220] M. J. Jaffe, A. W. Galston, *Annu. Rev. Plant Physiol.* **1968**, *19*, 417.

[221] C. G. Meloche, J. P. Knox, K. C. Vaughn, *Planta* **2007**, *225*, 485.

[222] M. H. Godinho, J. P. Canejo, L. F. V. Pinto, J. P. Borges, P. I. C. Teixeira, *Soft Matter* **2009**, *5*, 2772.

[223] P. E. S. Silva, F. Vistulo De Abreu, M. H. Godinho, *Soft Matter* **2017**, *13*, 6678.

[224] D. Li, Y. Xia, *Nano Lett.* **2004**, *4*, 933.

[225] G. Wang, D. Yu, R. V. Mohan, S. Gbewonyo, L. Zhang, *Compos. Sci. Technol.* **2016**, *129*, 19.

[226] D. Li, Y. Xia, *Adv. Mater.* **2004**, *16*, 1151.

[227] J. Doshi, D. H. Reneker, *J. Electrostat.* **1995**, *35*, 151.

[228] D. H. Reneker, A. L. Yarin, *Polymer* **2008**, *49*, 2387.

[229] P. Katta, M. Alessandro, R. D. Ramsier, G. G. Chase, *Nano Lett.* **2004**, *4*, 2215.

[230] K. W. Kim, K. H. Lee, M. S. Khil, Y. S. Ho, H. Y. Kim, *Fibers Polym.* **2004**, *5*, 122.

[231] R. R. Jose, R. Elia, M. A. Firpo, D. L. Kaplan, R. A. Peattie, *J. Mater. Sci. Mater. Med.* **2012**, *23*, 2679.

[232] S. Chen, H. Hou, P. Hu, J. H. Wendorff, A. Greiner, S. Agarwal, *Macromol. Mater. Eng.* **2009**, *294*, 781.

[233] S. Chen, H. Hou, P. Hu, J. H. Wendorff, A. Greiner, S. Agarwal, *Macromol. Mater. Eng.* **2009**, *294*, 265.

[234] C. Li, J. Wang, B. Zhang, *J. Appl. Polym. Sci.* **2012**, *123*, 2992.

[235] P. E. S. Silva, J. L. Trigueiros, A. C. Trindade, R. Simoes, R. G. Dias, M. H. Godinho, F. V. de Abreu, *Sci. Rep.* **2016**, *6*, 23413.

[236] A. C. Trindade, J. P. Canejo, P. I. C. Teixeira, P. Patrício, M. H. Godinho, *Macromol. Rapid Commun.* **2013**, *34*, 1618.

[237] W. Wang, C. Li, M. Cho, S. H. Ahn, *ACS Appl. Mater. Interfaces* **2018**, *10*, 10419.

[238] Y. Abraham, R. Elbaum, *New Phytol.* **2013**, *199*, 584.

[239] A. P. C. Almeida, L. Querciagrossa, P. E. S. Silva, F. Gonçalves, J. P. Canejo, P. L. Almeida, M. H. Godinho, C. Zannoni, *Soft Matter* **2019**, *15*, 2838.

[240] Y. Abraham, Y. Dong, A. Aharoni, R. Elbaum, *Cellulose* **2018**, *25*, 3827.

[241] Y. Abraham, C. Tamburu, E. Klein, J. W. C. Dunlop, P. Fratzl, U. Raviv, R. Elbaum, *J. R. Soc. Interface* **2012**, *9*, 640.

[242] D. Evangelista, S. Hotton, J. Dumais, *J. Exp. Biol.* **2011**, *214*, 521.

[243] W. Jung, W. Kim, H. Y. Kim, *Integr. Comp. Biol.* **2014**, *54*, 1034.

[244] D. Luo, A. Maheshwari, A. Danielescu, J. Li, Y. Yang, Y. Tao, L. Sun, D. K. Patel, G. Wang, S. Yang, T. Zhang, L. Yao, *Nature* **2023**, *614*, 463.

Biographies

Rafaela R. da Rosa received her B.Sc. (2011), M.Sc. (2013), and Ph.D. in Chemistry (2018) at the Universidade Federal do Rio Grande do Sul, Brazil. She worked as a temporary Professor in the Physical Chemistry Department at the same Institution (2013). She was a visiting Ph.D. student in 2017 at the University of Colorado Boulder, USA. She joined the Soft and Biofunctional Materials Group in 2018, working at the Materials Science Department, NOVA School of Science and Technology, NOVA University Lisbon, Portugal. Rafaela is a postdoctoral researcher developing new technologies from cellulose and its derivatives.

Susete N. Fernandes received her Ph.D. in Chemical Engineering from Instituto Superior Técnico (UL, PT) with an emphasis on polymer science. In November 2010 she joined the group of Soft and Biofunctional Materials Group from i3N/CENIMAT, Materials Science Department of NOVA School of Science and Technology, NOVA University Lisbon, Portugal. In 2023, she was invited to join the department as an assistant professor. In recent years, she has devoted her research interest to bio-based materials, mainly from cellulose nanocrystals, derived from liquid crystalline phases to produce optical, mechanical responsive systems.

Michel Mitov is director of research at the French National Centre for Scientific Research (CNRS). His current research interests include twisted liquid crystal design, optics and structure, and their biomimetic versions inspired by insect carapaces. He is the inventor of patents for smart windows that manage solar light and temperature. He wrote the book *Sensitive Matter*, which is a scientific essay about soft matter.

Maria Helena Godinho has D.Sc. and Ph.D. degrees in materials science and a Graduation in chemical engineering. During her Ph.D., she was a Nato/Invotan fellow in France. From 2016 to 2020, she was the vice president of the International Liquid Crystal Society. She received the 2019 Freéderiksz Medal of the Russian Liquid Crystal Society and the 2023 Lars Onsager Professorship and Medal, sponsored by the Norwegian University of Science and Technology. She is a professor with a habilitation in Materials Science at NOVA University Lisbon. Her research mainly focuses on functional materials inspired by nature based on cellulose and liquid crystalline systems.